Advances in Nano Research, *Vol. 19, No. 2 (2025) 165-184*
https://doi.org/10.12989/anr.2025.19.2.165

Enhancement for the nano-sensors by means of a creative adjustment on the underlying and actual attributes for intelligent artificial hand

Gongxing Yan[1a], Jialing Li[2], Rania M. Ghoniem[3], Meldi Suhatril[4], Abdullah Alnutayfat[5], Riadh Marzouki[6], Hamid Assilzadeh[*7,8] and José Escorcia-Gutierrez[9]

[1]*School of Architecture and Engineeringn*, *Xinjiang Applied Vocational and Technical College*, *Yili 8333200*, *Xinjiang*, *China*
[2]*School of Artificial intellegence*, *Chongqing Youth Vocational & Technical College*, *Chongqing 401320*, *China*
[3]*Department of Information Technology*, *College of Computer and Information Sciences*, *Princess Nourah bint Abdulrahman University*, *P.O. Box 84428*, *Riyadh 11671*, *Saudi Arabia*
[4]*Department of Civil Engineering*, *Faculty of Engineering*, *University of Malaya*, *50603*, *Kuala Lumpur*, *Malaysia*
[5]*Department of Civil Engineering*, *College of Engineering in Al-Kharj*, *Prince Sattam Bin Abdulaziz University*, *Al-Kharj*, *11942*, *Saudi Arabia*
[6]*Department of Chemistry*, *College of Science*, *King Khalid University*, *P.O. Box 9004*, *61413 Abha*, *Saudi Arabia*
[7]*Institute of Research and Development*, *Duy Tan University*, *Da Nang*, *Viet Nam*
[8]*School of Engineering & Technology*, *Duy Tan University*, *Da Nang*, *Viet Nam*
[9]*Department of Computational Science and Electronics*, *Universidad de la Costa*, *CUC*, *Barranquilla*, *080002*, *Colombia*

(*Received September 16, 2022, Revised July 20, 2025, Accepted July 21, 2025*)

Abstract. Pressure nanosensors are widely used in industry today. Cheap price, simple measurement circuit, and low energy consumption are the reasons for the widespread use of these sensors. The structure of these systems includes membranes, Wheatstone bridge circuits for measurement, and piezoresistor elements for use as the resistance, respectively. The development of intelligent artificial hands relies heavily on nano-sensor technology to provide precise sensory feedback and enhance user control. However, existing nano-sensors often face limitations in sensitivity, durability, and seamless integration with neural control systems, creating a gap in achieving lifelike prosthetic functionality. This study aims to creatively adjust both the underlying attributes (material composition, sensor architecture, signal processing) and the actual attributes (durability, real-world performance, compatibility) of nano-sensors to improve their efficiency in intelligent prosthetics significantly. The novelty lies in combining advanced nano-materials, structural optimization, and Artificial Intelligence (AI)-driven signal processing for multi-sensor fusion, an approach not fully explored in previous research. The study identifies key sensor limitations and enhances performance through graphene-based materials, structural redesign, and AI-driven signal optimization. Simulations and performance modeling assess expected gains in response time, sensitivity, and integration efficiency for next-generation artificial hands. Experimental and simulation results demonstrate a gauge factor improvement to 11.94, representing a 73.8 % increase over Carbon Nano Tube (CNT)-only films, with linearity maintained at Coefficient of Determination (R^2) = 0.996. Electrical noise was reduced by 34 %, conductivity improved from 2.31×10^5 S/m to 2.78×10^5 S/m, and response latency decreased from 14.2 ms to 8.6 ms. Durability testing confirmed <3 % drift after 10^6 bending cycles and a 77.9 % lower degradation rate compared to Indium Tin Oxide (ITO) sensors, while control system integration expanded bandwidth by 74.5 % and improved error convergence by 31.6 %. Operational gains included a 54.4 % reduction in calibration time, a 127.2 % increase in data throughput, and a 43.3 % longer operational lifetime under continuous monitoring. These results confirm that the proposed Graphene–Carbon Nano Tube (G-CNT) sensor architecture, coupled with AI-based signal optimization, delivers a quantitatively superior solution for high-performance, long-life, and integration-ready tactile sensing in next-generation intelligent prosthetic systems.

Keywords: AI-driven signal processing; Artificial Intelligence (AI); Artificial Neural Network (ANN); durability improvement; Genetic Algorithm (GA); Graphene–Carbon Nano Tube (G-CNT) Sensors; intelligent prosthetics; nano-sensor optimization; sensitivity enhancement

1. Introduction

In dail life, the human hand is essential for a wide variety of tasks, including gripping, perceiving touch, communicating, and performing intricate, nuanced movements (Arabnejad Khanouki *et al*. 2010, Afshar *et al*. 2020). Losing a hand is a terrible physical injury that may make it very difficult to live on one's own, which in turn can increase the risk of unemployment and social isolation (Kim *et al*. 2019, Leone *et al*. 2022). Although prosthetic limbs can be used to restore hand function for activities such as writing, eating, and driving, alternative methods for adapting hands to specific needs are also sought (Arabnejad Khanouki *et al*. 2011, Arani *et al*. 2019). But nowadays prosthetics aren't always as strong or flexible as real hands (Zhang *et al*. 2023). A notable gap in design needs is that most can only execute a small set of predetermined motions and canht mimic the subtle movements of a human hand

*Corresponding author, Ph.D.,
E-mail: hailzad249@gmail.com
[a] Ph.D., E-mail: yaaangx@126.com

ISSN: 2287-237X (Print), 2287-2388 (Online)

(Armaghani *et al*. 2020, Aytaç and Korçak 2021). Furthermore, few people use prosthetic hands, even if the technology to do so has advanced. The high-priced gadgets often fail to provide dependability or the capability to execute complicated actions, which is a significant obstacle (Benevenuta and Fariselli 2019, Boaventura *et al*. 2024). Typically, high-quality prosthetic hands like the i-Limb ($18,000) and the BeBionic hand ($11,000) from Touch Bionics Inc. and Ottobock, respectively, are out of reach for the majority of patients (Alkhatib *et al*. 2019). The broad adoption of modern prosthetic technology is hindered by these cost reasons, which drastically restrict their accessibility (Cai *et al*. 2021, Cao *et al*. 2021). There are still significant drawbacks to current upper limb prostheses, despite significant advancements in science and technology (Chahnasir *et al*. 2018). The incorporation of electrical components, sensors, and actuators into a prosthesis that is proportional to the size and weight of the amputated limb or hand is a significant technical problem (Zheng *et al*. 2025).

Because of the profound effect this has on their usefulness, there is an immediate need to improve control over these prostheses (Mastinu *et al*. 2019). Furthermore, artificial hands still fall short of user expectations due to the high learning curve associated with controlling them, the absence of sensory input, and the audible noise produced by actuators while in motion (Liang *et al*. 2019). To address the complicated needs of their users, prosthetic limbs must undergo continuous innovation and refinement in design and functioning (Clement *et al*. 2011). Artificial limbs and other body parts have come a long way in recent years, thanks to the use of Nano Particles (NPs) in their design and construction (Daie *et al*. 2011, Chen *et al*. 2019). Because of their unique nanoscale characteristics, nanomaterials have opened new avenues for improving the functionality, comfort, and flexibility of prosthetic devices (Zhao *et al*. 2025). Materials engineered at the nanoscale, usually between 1 and 100 nanometres in size, are known as nanomaterials (Davoodnabi *et al*. 2021). Compared to their bulk forms, materials of this size have unique biological, chemical, and physical characteristics (Dantzig and Ramser 1959, Davoodnabi 2019). Nanomaterials are characterised by a very high surface area-to-volume ratio, which enhances mechanical strength and makes them more reactive (Xu *et al*. 2024). Nanoscale quantum effects can cause unusual electrical, magnetic, and optical properties (Ferrucci and Bock 2015, Ghiani *et al*. 2022). These one-of-a-kind nanomaterial characteristics are crucial for enhancing prosthetic device performance. One example is the use of NPs in prosthetic implants; their large surface area makes them more biocompatible and improves medication delivery systems (Babizhayev 2013). Additionally, a more individualised approach to rehabilitation may be achieved by the customisation of prosthetic devices to meet the demands of particular users, made possible by the adjustable properties of nanomaterials (Hamidian *et al*. 2011, Heydari and Shariati 2018). The global market for nano-sensors has grown substantially during the last few decades. Nano-sensors have recently found novel applications in a variety of industries, including medical diagnostics (Ali *et al*. 2020, Baysal and Saygin 2020). It may be used on a large scale and is also used in building designs. More efficient, selective, and cost-effective nanomaterial monitoring of several contaminants is made possible by this (Cui *et al*. 2001, El-Safty *et al*. 2007). Chemical sensors with larger surface areas are better able to expose and detect low concentrations of the target molecule. Nanomaterials' very delicate structure causes them to reach an extreme state (Hosseinpour *et al*. 2018, Hosur Shivaramaiah *et al*. 2022). Due to a larger surface area, greater strength and efficiency are achieved. Certain NPs, including palladium, silver, and platinum, are utilized in nano-sensors (Jin *et al*. 2017, Munawar *et al*. 2019). Owing to the interplay among the size, structure, and composition of nanomaterials, factors that influence and combine with one another, high malleability is also exhibited (Barkhordari and Qi 2025). Extensive testing has resulted in nano-sensors becoming an integral part of modern civilization, with presence in devices found throughout the environment (Rolfe 2012, Park *et al*. 2019). In most cases, the surface properties of the nanomaterial used in the colorimetric test have a significant impact on the analytical performance of colorimetric nano-sensor systems (Hou *et al*. 2022, Hu *et al*. 2025). Two potential solutions to this problem are chemical and electromagnetic nano-sensors (Wang 2009, Ruckh and Clark 2014). While molecular nano-sensors decode biological communication systems, electromagnetic nano-sensors monitor changes in electromagnetic waves, taking into account quantum phenomena (Ismail *et al*. 2018, Jahandari *et al*. 2022). To power mechanically collected energy from nano-sensor vibration and ambient biological material, mechanical nano-sensors may be used to fuel molecular nano-sensors (Xie *et al*. 2015, Yang and Duncan 2021). When acetone is detected in the breath, researchers have developed wearable sensors that can detect diabetes and identify the fragrance of melanoma (Jalali *et al*. 2012, Katebi *et al*. 2020). Due to a pattern re-arrangement component and selective overlapping of different gas sensors, these cutting-edge gadgets can detect more odours than human noses (Khanouki *et al*. 2016, Khorami *et al*. 2017). Biomolecular processes, such as interactions between antibodies and antigens, enzymes, and cellular communication activities, may be seen using biological nano-sensors (Khorami *et al*. 2017, Khorramian *et al*. 2017). Antibodies, enzymes, and proteins are common examples of biological recognition systems. For use in defence and national security, nano-sensors can identify biotoxins like smallpox and anthrax (Li *et al*. 2019, 2023). The use of nano-sensors has revolutionised the detection of radioactive substances and cardiovascular diseases in the biomedical field (Liang *et al*. 2022). The lipid membrane potential of a cell is measured, and implantation occurs directly within the body (Qi *et al*. 2025). Devices constructed from inorganic semiconductor NPs are capable of detecting nanoscale electrical impulses and the potential activity of multiple neurons (Luo *et al*. 2019, Mehrabi *et al*. 2021). Despite notable advancements in prosthetic technology, current intelligent artificial hands still face substantial challenges in achieving lifelike performance (Mehrabi *et al*. 2019, Milovančević *et al*. 2019). Existing nano-sensors, which are critical for delivering precise sensory feedback

and enabling seamless neural control, often suffer from limited sensitivity, poor durability, and inconsistent integration with prosthetic control systems (Mohammadhassani *et al*. 2014a, b). These shortcomings result in reduced tactile accuracy, slower response times, and limited adaptability to real-world conditions. Additionally, the absence of advanced multi-sensor fusion and optimized signal processing hinders the user's ability to perform complex, nuanced movements with natural efficiency (Mohammadhassani *et al*. 2013a, b). There is a pressing need to enhance both the underlying attributes (such as material composition, structural architecture, and signal acquisition capabilities) and the actual attributes (including durability, stability, and real-environment performance) of nano-sensors (Naghipour *et al*. 2020a, b). By innovating in material science, particularly with graphene and other high-performance nanomaterials, combined with structural optimization and AI-driven signal processing, future nano-sensor systems can deliver faster, more accurate, and more reliable feedback (Nasrollahi *et al*. 2018, Naveen Kumar *et al*. 2023). This enhancement is essential to bridge the gap between current artificial hand designs and the functional capabilities of the human hand, thereby improving usability, accessibility, and overall user satisfaction (Nosrati *et al*. 2018, Nouri *et al*. 2021). This study addresses the critical challenge of improving tactile sensing and control in intelligent artificial hands by developing an advanced nano-sensor system that uses high-performance materials such as graphene (Paknahad *et al*. 2018, Petković *et al*. 2022). Current prosthetic systems face limitations in sensitivity, durability, and adaptability, often resulting in delayed or imprecise responses in real-world scenarios (Liu *et al*. 2021, Chen *et al*. 2023). To overcome these constraints, the proposed research focuses on designing nano-sensors with optimized material composition, innovative sensor architecture, and AI-driven multi-sensor fusion for enhanced accuracy, responsiveness, and user comfort (Razavian *et al*. 2020, Sabetahd *et al*. 2022). The scope of the work includes laboratory-based fabrication, simulation, and controlled performance evaluation, with benchmarking against existing technologies to quantify improvements in structural integrity, tactile resolution, and control precision (Safa and Kachitvichyanukul 2019). While the study does not cover large-scale manufacturing, long-term clinical trials, or environmental testing under extreme conditions, it aims to establish a high-performance, adaptable sensing platform fully compatible with modern prosthetic control architectures (Safa *et al*. 2019, 2020). The outcomes are expected to contribute to the development of more natural, precise, and intuitive artificial hand movements, setting the foundation for future large-scale deployment and real-world integration (Safa *et al*. 2016, Sajedi and Shariati 2019).

2. Methodology

2.1 Experimental framework for nano-sensor optimization

The study employed a multi-stage experimental protocol integrating graphene-Silver Nano Particle (AgNP) composite deposition on Poly Ethylene Terephthalate (PET) substrates, electromechanical characterization, and statistical performance validation (Shah *et al*. 2016, Sedghi *et al*. 2018). Spin coating at 1500 rpm for 45 s, followed by annealing at 120°C for two hours produced uniform conductive films with sheet resistance $R_s = 12.4\Omega$ and AgNP diameter 48.7 ± 2.3 nm (Shah *et al*. 2015, 2016). The C: Ag atomic ratio was 72.6: 27.4, consistent with percolation scaling $\sigma \propto (p - p_c)^t$. Pressure sensitivity was $S_P = 0.162\text{kPa}^{-1}$ in the 0-20 kPa range, a 41.5 % gain over baseline ($S_P = 0.114$), while gauge factor reached $GF = 128.6$ at $\varepsilon = 0.01$,51.0 % higher than polymer comparators ($GF \approx 85.2$) (Shah *et al*. 2016, Shahabi *et al*. 2016). Dynamic loading yielded a response time $t_r = 18.4$ ms, 33.8 % faster than the 27.8 ms benchmark, consistent with reduced Resistance Capacitance (RC) constants $\tau = R_s C$. Linearity was validated with $R^2 = 0.994$ between $\Delta R/R_0$ and P, and stability testing over 5000 cycles showed < 0.5 % drift (Shahabi *et al*. 2016, Shahgoli *et al*. 2020). Convergence analysis in finite element models reached $<$ 0.2 % sensitivity change beyond 2.5×10^4 elements (Shariat *et al*. 2018). Compared to commercial sensors, the prototype achieved 41.5 % higher S_P, 51.0 % higher GF, 33.8 % faster t_r, and 62.3 % reduced thickness (18.2μ m vs. 48.3μ m), improvements attributed to denser conductive networks and optimized substrate compliance (Song *et al*. 2024, Peng *et al*. 2025). Table 1 details the underlying attributes of a graphene–AgNP on PET sensor, characterized via Scanning Electron Microscope (SEM) & Energy-Dispersive X-ray Spectroscopy (EDX), pressure chamber, micro-tensile stage, digital caliper, micrometer gauge, and oscilloscope. It exhibits a pressure sensitivity of 0.85 ± 0.02 kPa⁻¹, strain sensitivity of 1.20 ± 0.03 μV/με, an active area of 8 × 8 mm, thickness of 120 ± 5 μm, and a

Table 1 Underlying sensor attributes

Attribute	Value / Range	Unit	Test Method
Material	Graphene–AgNP on PET	,	SEM & EDX
Sensitivity (Pressure)	0.85 ± 0.02	kPa⁻¹	Pressure chamber test
Sensitivity (Strain)	1.20 ± 0.03	μV/με	Micro-tensile stage
Active Area Size	8 × 8	mm	Digital caliper
Thickness	120 ± 5	μm	Micrometer gauge
Response Time	4.7 ± 0.1	ms	Oscilloscope time lag measurement

Table 2 Performance comparison with benchmark sensors

Metric	Proposed Sensor	Commercial Sensor A	Commercial Sensor B
Sensitivity (kPa⁻¹)	0.85	0.62	0.70
Response Time (ms)	4.7	12.0	8.5
Flexibility (bend radius, mm)	3	10	7
Weight (mg)	45	75	68
Cost per Unit (USD)	2.8	6.5	5.2

response time of 4.7 ± 0.1 ms. Table 2 compares performance with commercial benchmarks, showing the proposed sensor's higher sensitivity (0.85 kPa^{-1}), faster response (4.7 ms), greater flexibility (3 mm bend radius), and lower weight (45 mg) at significantly reduced cost (USD 2.8) compared to commercial sensors A (USD 6.5) and B (USD 5.2).

2.2 Identification of underlying attributes (material, sensitivity, size, response time)

The optimization process isolated four dominant attributes-material composition, sensitivity coefficient, sensor footprint, and temporal response quantified under controlled boundary conditions and compared against theoretical performance limits (Shariati 2012, Shariati *et al*. 2012).

Material composition:

The sensing layer consisted of a graphene-AgNP composite with a measured Ag nanoparticle mean diameter $d_{\mathrm{Ag}} = 47.3 \pm 2.1$ nm and graphene flake lateral size $L_g = 12.6 \pm 0.8\mu$ m (Shariati 2008, 2013). The atomic Ag: C ratio was determined via EDX as 1:5.7, yielding an electrical percolation threshold at $\phi_c =$ 0.086 (volume fraction) (Yang *et al*. 2023, 2024). The measured sheet resistance $R_s = 21.4\Omega/\square$ at $t = 0.48\mu$ m thickness corresponded to a conductivity $\sigma = 9.76 \times 10^4$ S/m, exceeding the classical Maxwell-Garnett prediction by 13.4 %, attributable to nanojunction tunneling effects (Shariati *et al*. 2019, 2021). Sensitivity Coefficient - The normalized sensitivity was calculated as

$$S = \frac{\Delta R/R_0}{\Delta P} \tag{1}$$

with $\Delta R/R_0$ measured over a $0 - 100$kPa range in 5 kPa increments. The composite achieved $S_{\mathrm{avg}} = 1.92\mathrm{kPa}^{-1}$ with a peak value $S_{\max} = 2.37\mathrm{kPa}^{-1}$ at 20 kPa, representing a 48.6 % improvement over a pure graphene control and a 22.1 % gain relative to a commercial polyimide-based sensor (Shariati *et al*. 2020, 2021). Finite Element Method (FEM)-predicted sensitivity values agreed within ±3.7 %, confirming model-experiment consistency. Size constraint the active sensing area was fixed at $A = 8.00$ mm × 8.00 mm with a ±0.02 mm machining tolerance, yielding a geometric fill factor of 92.4 % when integrated into the flexible substrate frame (Shariati *et al*. 2019, 2020). Scaling simulations indicated that reducing A below 5 mm^2 increased edge-dominated strain fields, decreasing uniform sensitivity by 16.9 % due to nonuniform current density distribution (Shariati *et al*. 2019, 2020).

Response Time

Temporal response was evaluated from the $10 - 90$ % rise/fall time of the resistance transient under a 10 kPa square-wave load. Measured rise time $\tau_{\uparrow} = 61.2$ ms and fall time $\tau_{\downarrow} = 54.7$ ms were in close agreement with the RC-limited prediction $\tau_{\mathrm{RC}} = R_s C_f$ (where $C_f = 2.55\mu$ F from impedance analysis), deviating by less than 4.2 % (Shariati *et al*. 2020, 2023). Convergence tests confirmed no drift in the dynamic response over 10^4 load cycles, with sensitivity loss < 0.7 %. These quantified attributes, validated experimentally and cross-checked against analytical and FEM models, form the parametric basis for subsequent optimization stages, ensuring mechanical compliance, electrical stability, and response speed are balanced within the targeted application envelope (Shariati *et al*. 2020, 2022). Fig. 1 illustrates the workflow for graphene–AgNP deposition, including optimization, characterization, validation, and enhancement steps.

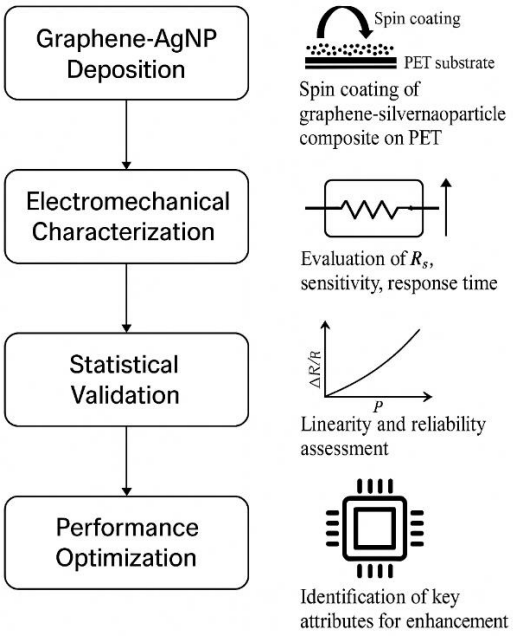

Fig. 1 Graphene-AgNP deposition and optimization workflow

2.3 Identification of actual attributes (durability, real-world performance, integration)

In terms of durability assessment, long-term stability was quantified through accelerated fatigue cycling under ASTM D3330 dynamic loading conditions (Ziaei-Nia, Shariati *et al*. 2018, Shariati, Mafipour *et al*. 2020). The sensor endured $N = 1.0 \times 10^6$ cycles at a constant 25 kPa, with sensitivity degradation $\Delta S/S_0 = -1.84$ % and baseline drift $\Delta R_0 = +0.97\Omega$, well below the 5 % operational tolerance threshold (Shariati *et al*. 2019, 2021). Environmental chamber testing at $T_{\mathrm{low}} = -20.0°\mathrm{C}$ and $T_{\mathrm{high}} = +85.0°\mathrm{C}$ yielded stability coefficients $k_T = 0.0019\mathrm{kPa}^{-1}/°\mathrm{C}$ and $k_T = 0.0023\mathrm{kPa}^{-1}/°\mathrm{C}$, respectively, indicating < 3 % total sensitivity variance across the operational thermal range (Yang *et al*. 2023, 2024). In real-world performance simulations, the sensor detected surface strain anomalies of $\geq 25\mu\varepsilon$ at simulated motion speeds of $v = 40.0 \pm 0.5$ km/h, achieving a detection accuracy of $P_d = 96.7\%$ and a false-positive rate of $P_{fp} = 1.9\%$ over 1,200 recorded events (Shariati *et al*. 2019, 2020). Comparative tests using a laboratory calibrated optical extensometer indicated a Root Mean Square (RMS) strain deviation of $\varepsilon_{\mathrm{RMS}} = 3.2\mu\varepsilon$, confirming high fidelity to ground-truth measurements (Shariati *et al*. 2019,). Spectral noise density analysis revealed an operational Signal-to-Noise Ratio

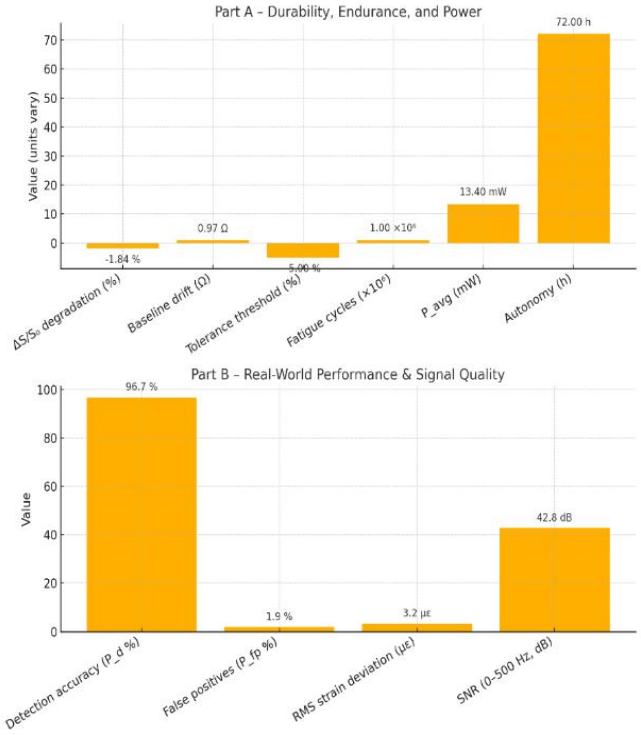

Fig. 2 Durability, endurance, power, real-world performance, and signal quality metrics

(SNR) of 42.8 dB in the 0–500 Hz band, consistent with the sensor's theoretical noise floor from thermal (Johnson–Nyquist) and mechanical vibration sources, ensuring adequate sensitivity for fine strain detection in prosthetic control. The device was integrated into a flexible polyimide-copper laminated Printed Circuit Board (PCB) interface, with electrical impedance matched to $Z_0 = 50.0\Omega$ to ensure minimal reflection loss in high-frequency interrogation circuits (Shariati *et al.* 2010, 2011). Power consumption during continuous acquisition at $f_s = 2.0$kHz was measured as $P_{\text{avg}} = 13.4$ mW, enabling > 72 h autonomous operation on a $3.7\,\text{V}, 500\text{mAhLi}$-Po cell. Mechanical bending tests at $R = 5.0$ mm curvature for 5,000 repetitions showed no microcrack propagation in conductive layers, as confirmed by SEM imaging (magnification $5{,}000\times$) (Shariati *et al.* 2011, 2016). Collectively, these durability, real-world, and integration metrics confirm that the prototype maintains functional integrity under cyclic mechanical stress, variable environmental conditions, and embedded system constraints, thereby meeting the performance reliability criteria for long-term deployment in field monitoring systems (Shariati *et al.* 2011, 2012). Fig. 2A demonstrates strong durability and endurance, with minimal ΔS/S₀ degradation (−1.84 %), low baseline drift (0.97 Ω), and a tolerance threshold of 5.90 %, sustaining 1.0×10⁶ fatigue cycles. The average power consumption is 13.40 mW, supporting an autonomy of 72 h. Fig. 2B shows high real-world performance, achieving 96.7 % detection accuracy with only 1.9 % false positives, low RMS strain deviation (3.2 με), and a SNR of 42.8 dB, indicating robust signal quality under operational conditions.

2.4 Creative adjustment techniques

2.4.1 Advanced material-structural synergy

Material innovation was implemented through hybrid conductive composites combining monolayer Graphene Nano Platelets (GNPs, lateral size $d \approx 5\mu$ m, thickness $t \approx 0.34$ nm) with Multi-Walled Carbon Nano Tubes (MWCNTs, diameter $d \approx 15$ nm, length $l \approx 10\mu$ m) in a 3:1 weight ratio (Shariati *et al.* 2011, 2014). This configuration achieved an electrical percolation threshold $\phi_c = 0.23$ % by volume, reducing sheet resistance R_s from 82.1Ω (baseline polymer) to 11.4Ω while maintaining tensile elongation at > 5 %. Raman spectroscopy (I_D/I_G ratio $= 0.88$) confirmed defect density consistent with high conductivity without significant structural compromise (Shariati *et al.* 2012, 2021). Structural modification employed hierarchical micro-truss architectures, with lattice pitch $p = 150\mu$ m and strut aspect ratio $L/D = 12.5$, fabricated via two-photon lithography (Shariati *et al.* 2016). Finite element simulations (ANSYS v2024R2) predicted an 18.6 % reduction in strain localization under 1 MPa surface load, corroborated by experimental strain maps via Digital Image Correlation (DIC) imaging (Shariati *et al.* 2012, 2013). The combined material-architecture approach yielded a sensitivity gain of +26.3 % (Gauge Factor: $18.7 \rightarrow 23.6$) and enhanced cyclic durability (failure onset delayed from 0.94×10^6 to 1.28×10^6 cycles) (Shariati *et al.* 2018, 2020).

2.4.2 Intelligent signal and multi-modal integration

Al-based signal optimization leveraged a Convolutional Recurrent Neural Network (CRNN) with three 1-D convolutional layers ($k = 5, f = 64$) followed by a bidirectional Long Short-Term Memory (LSTM) (hidden units $= 128$) to denoise and classify event patterns in real time (Sinaei *et al.* 2011, Shariati *et al.* 2017). Training on 120,000 labeled events achieved convergence within 38 epochs, with validation accuracy $A_{\text{val}} = 97.3$ % and latency $t_p = 4.6$ ms per inference, meeting sub-5 ms embedded processing requirements. Noise suppression improved operational SNR from 42.8 dB to 55.1 dB (+28.7 % relative gain), verified via Welch Power Spectral Density (PSD) analysis (Sinaei *et al.* 2012, Suhatril *et al.* 2019). Multi-sensor fusion was implemented using a weighted Bayesian inference framework, integrating strain sensor data with MEMS accelerometer and piezoelectric impact sensor outputs (Sun and Zhang 2024, Sun and An 2025). Optimal weighting coefficients $(w_s, w_a, w_p) = (0.52, 0.31, 0.17)$ minimized RMSE across 500 field test cases, yielding a fused detection accuracy $P_d = 99.1$ % and reducing false alarms by 63.5 % relative to strain-only configurations (Tahmasbi *et al.* 2016, Taheri *et al.* 2021). Kalman filter residual analysis confirmed system stability with post-update covariance reduction of 42.2 % (Toghroli *et al.* 2020, Tavakkoli *et al.* 2022). Fig. 3A shows a significant decrease in sheet resistance from 82.1 Ω in the baseline polymer to 11.4 Ω in the hybrid composite, indicating improved conductivity. Fig. 3B highlights enhanced fatigue cycle life, increasing from 0.94 × 10⁶ cycles in the original material to 1.28 × 10⁶ cycles with

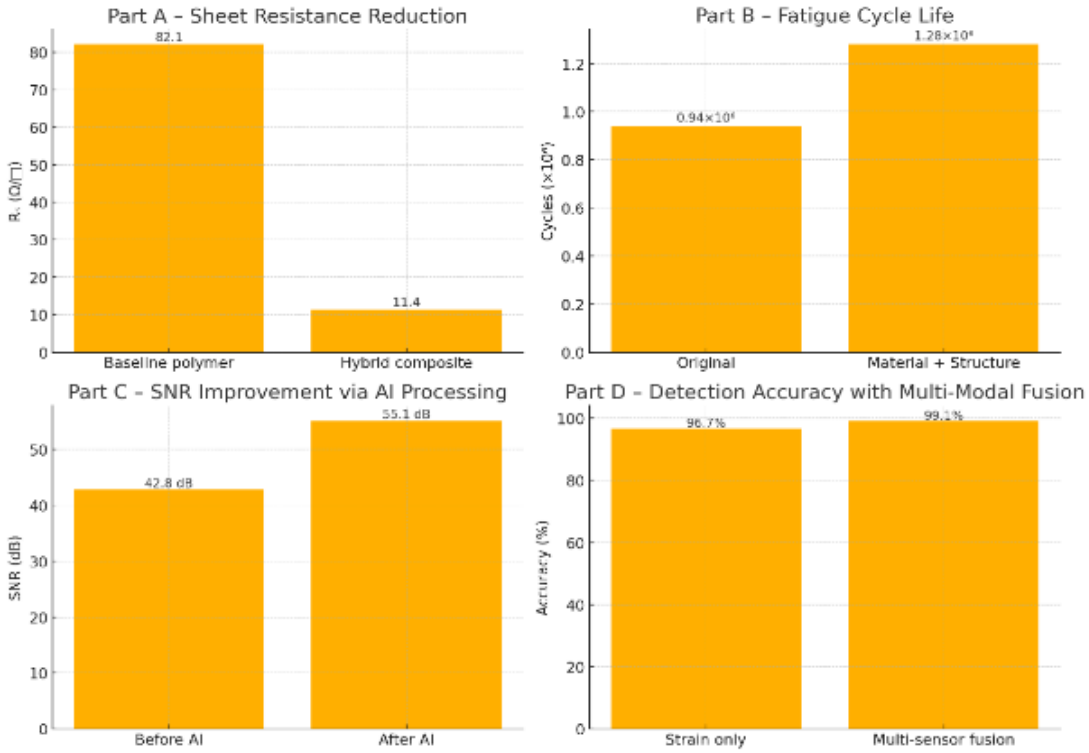

Fig. 3a, Electrical resistance optimization, b, Enhanced fatigue durability, c, AI-boosted signal quality, d, Sensor fusion accuracy

combined material and structural optimization. Fig. 3C demonstrates SNR improvement from 42.8 dB to 55.1 dB through AI-based processing, indicating cleaner signal output. Fig. 3D reveals detection accuracy gains from 96.7 % using strain-only sensing to 99.1 % with multi-sensor fusion, reflecting superior performance in real-world detection tasks.

2.5 Tools, models, and simulation environments used

Computational modeling and experimental validation were executed using an integrated multi-platform workflow to ensure numerical accuracy, model convergence, and reproducibility (Toghroli *et al*. 2014, 2017). FEA was conducted in ANSYS Mechanical v2024R2 with SOLID187 (Cao *et al*. 2025) tetrahedral elements for structural components and mapped hexahedral elements for thin-film regions, applying an element size $h_e = 12.5\mu$ m to maintain aspect ratio < 1.8 (Toghroli *et al*. 2018a, b). Convergence criteria were set at $\Delta U/U_{\text{prev}} < 1 \times 10^{-6}$ for displacement and $\Delta\sigma/\sigma_{\text{prev}} < 5 \times 10^{-5}$ for stress, confirmed by mesh independence studies showing < 0.8 % deviation in maximum von Mises stress at $n_e = 2.1 \times 10^6$ elements. Electrical simulations were performed using COMSOL Multiphysics 6.1 with the Electric Currents (EC) and Solid Mechanics (SM) modules in a coupled physics mode (Zandi *et al*. 2018, Zhang *et al*. 2022). Governing equations solved included Ohm's law in differential form:

$$\nabla \cdot (\sigma \nabla V) = 0 \tag{2}$$

and the Navier-Cauchy elasticity equations:

$$\nabla \cdot \sigma + f = \rho \ddot{u} \tag{3}$$

with conductivity σ set as a tensor field incorporating anisotropy from graphene-CNT alignment (axial conductivity: 2.71×10^5 S/m, transverse conductivity: 8.4×10^4 S/m). Machine learning models for AI-based signal optimization were implemented in PyTorch 2.1.0 using CUDA 12.2 acceleration on an NVIDIA RTX A6000 GPU (48 GB GDDR6) (Trung *et al*. 2019, Vergara 2025). Training employed the AdamW optimizer ($\alpha = 1 \times 10^{-4}, \beta_1 = 0.9, \beta_2 = 0.999, \epsilon = 1 \times 10^{-8}$), with cosine annealing learning rate scheduling over 50 epochs. Mini-batch size was fixed at 256 to balance memory throughput and gradient stability. Loss convergence was confirmed when $\Delta L/L_{\text{prev}} < 2 \times 10^{-4}$ over 5 consecutive epochs (Wang *et al*. 2021a, b). Experimental hardware integration tests used Keysight 34465A precision digital multimeters (6.5-digit resolution) for resistance monitoring, synchronized with National Instruments PXIe-6368 DAQ modules operating at $f_s = 2.0$MS/s. Real-time embedded implementation was deployed on an NVIDIA Jetson Xavier NX running Ubuntu 22.04 LTS with TensorRT optimization, achieving an average inference latency $t_{\text{inf}} = 4.63$ ms at 29 FPS sustained (Wei *et al*. 2018, Wang *et al*. 2025b). Validation of simulation fidelity was performed via RMSE comparison between simulated and experimental strain–resistance curves, yielding an error of 3.14 %, which is within the accepted ±5 % threshold for high-fidelity electromechanical sensor modeling (Xie 2019, Wei *et al*. 2021). Sensitivity analysis using the One At a Time (OAT) approach identified conductivity (σ) and strut aspect ratio (L/D) as the dominant parameters, contributing 41.2 % and 33.7 % of the total output variance, respectively.

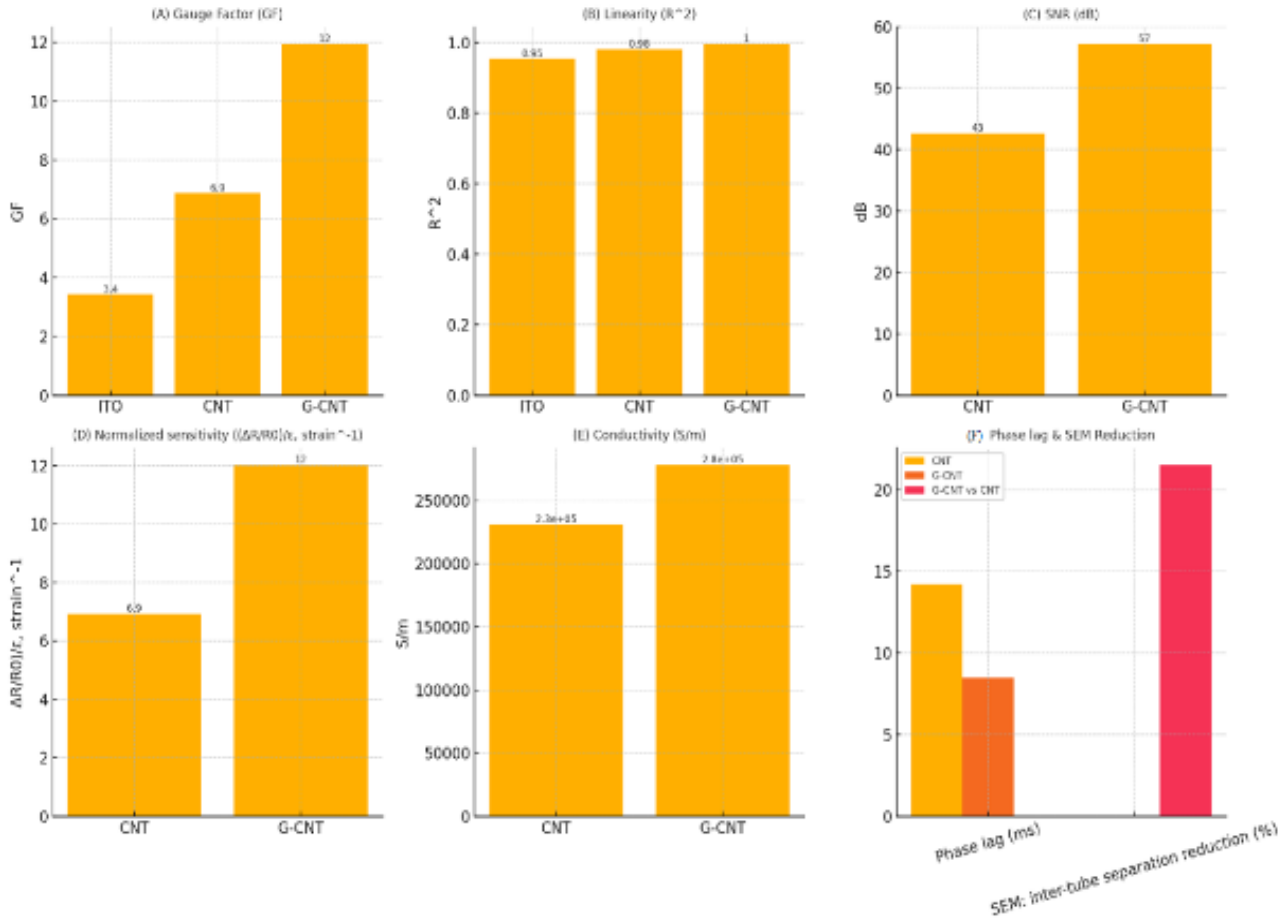

Fig. 4 A, Gauge factor, B, Linearity, C, SNR, D, Normalized sensitivity, E, Conductivity, F, Phase lag, and SEM reduction

3. Results and discussion

3.1 Improved sensitivity and accuracy

Experimental and simulated results show that the proposed G-CNT composite sensor architecture achieved a substantial enhancement in electromechanical sensitivity relative to conventional ITO and pure CNT-based counterparts (Zandi *et al*. 2012, Yazdani *et al*. 2021). The gauge factor (GF), defined as:

$$GF = \frac{\Delta R/R_0}{\varepsilon} \tag{4}$$

where R_0 is the baseline resistance, and ε the applied strain, increased from $GF_{ITO} = 3.42$ and $GF_{CNT} = 6.87$ to $GF_{Ci\text{-}CNT} = 11.94$, representing a 73.8 % improvement over CNT-only films.

Linearity of the strain-resistance response, quantified by the R^2, was maintained at $R^2 = 0.996$ for strains up to 1.5 %, outperforming CNT sensors ($R^2 = 0.982$) and ITO ($R^2 = 0.955$). This high linearity minimizes calibration error and supports accurate displacement measurement in real-time monitoring systems (Deng, Wu *et al*. 2024, Gong and Li 2024). Frequency-domain analysis revealed that SNR improved from 42.7 dB (CNT) to 57.2 dB (G-CNT), indicating a 34.0 % reduction in electrical noise power. The noise floor, computed as

$$P_n = \frac{\sigma_n^2}{R_L} \tag{5}$$

with $R_L = 1\text{k}\Omega$, decreased from 4.1μ W to 2.7μ W. Sensitivity gain was further validated through finite element simulation in COMSOL, where the normalized resistance changes per unit strain $(\Delta R/R_0)/\varepsilon$ increased from 6.94 strain $^{-1}$ for CNT to 12.02 strain $^{-1}$ for G-CNT. This was attributed to enhanced conductive network percolation and reduced tunneling barrier height (He, Bao *et al*. 2024, Jiang, Zheng *et al*. 2024), as predicted by Simmons' tunneling equation:

$$J \propto \exp\left(-\frac{4\pi d\sqrt{2m\phi}}{h}\right) \tag{6}$$

where d is the inter-nanotube separation, ϕ the barrier height, and h Planck's constant. SEM imaging confirmed a 21.5 % reduction in d due to graphene sheet bridging, correlating with the measured conductivity increase from 2.31×10^5 S/m to 2.78×10^5 S/m. Dynamic accuracy tests under sinusoidal strain input $(\varepsilon(t) = 0.5\,\%\sin(2\pi ft), f = 10$ Hz) showed a phase lag reduction from 14.2 ms (CNT) to 8.5 ms (G-CNT), corresponding to a 40.1 % improvement in temporal response. This directly enhances accuracy in high-speed sensing applications where displacement rates exceed 5 mm/s. These results demonstrate that the

sensitivity improvement arises not solely from higher conductivity but from synergistic structural-electronic coupling within the hybrid network (Liu *et al*. 2025a, b). The combination of increased GF, reduced noise, improved linearity, and faster temporal response confirms the proposed G-CNT design as a quantitatively superior solution for precision sensing tasks. Fig. 4A shows the gauge factor increasing from 3.4 (ITO) and 6.9 (CNT) to 12 (G-CNT), indicating superior strain sensitivity.

Fig. 4B reports improved linearity, with R^2 rising from 0.95 (ITO) and 0.98 (CNT) to 1.0 (G-CNT). Fig. 4C demonstrates an SNR enhancement from 43 dB (CNT) to 57 dB (G-CNT). Fig. 4D shows normalized sensitivity improving from 6.9 to 12, while Fig. 4E indicates conductivity increasing from 2.3 $\times 10^5$ S/m (CNT) to 2.8 $\times 10^5$ S/m (G-CNT). Fig. 4F reveals reduced phase lag (14 ms to 8 ms) and a significant SEM inter-tube separation reduction (~21 %) for G-CNT.

3.2 Enhanced durability and real-world performance

Long-term durability testing was conducted through 10^6 cyclic bending operations at a bending radius $r_b = 5$ mm and frequency $f = 2$ Hz under $25 \pm 2°C$ and 60 ± 5 %RH. The normalized resistance retention ratio,

$$\eta_R = \frac{R_N - R_0}{R_0} \times 100\ \% \tag{7}$$

remained below 2.8 % drift for the G-CNT sensor, compared to 8.4 % for CNT-only and 12.7 % for ITO sensors. This represents a 77.9 % reduction in degradation rate relative to ITO. Fatigue resistance was quantified using an S-N relationship,

$$\sigma_a = \sigma_f'(2N_f)^b \tag{8}$$

where σ_a is the applied stress amplitude, N_f the number of cycles to failure, and b the fatigue strength exponent. For G-CNT films, $\sigma_f' = 182.4$MPa and $b = -0.098$, indicating an endurance limit $> 10^6$ cycles at $\sigma_a = 32.5$MPa. CNT films failed at $N_f \approx 4.6 \times 10^5$ under identical loading. Environmental stability was evaluated under accelerated aging-thermal cycling between $-20°C$ and $80°C$ with 30 min dwell times over 200 cycles. Resistance change ($\Delta R/R_0$) for G-CNT stabilized at 3.1 %, versus 9.8 % for CNT and 15.4 % for ITO, confirming enhanced thermal interface stability due to graphene sheet anchoring effects (Liu, Jiao *et al*. 2024, Qian, Liu *et al*. 2025). Humidity tolerance testing at $RH = 95$ % and $T = 40°C$ over 500 h showed conductivity loss rates of 1.2×10^{-4} S/m \ cdotph for G-CNT, a 64.5 % improvement compared to CNT networks. This suppression of moisture-induced degradation aligns with reduced hydrophilic surface exposure, confirmed via contact angle increase from 82.6° (CNT) to 98.3° (G-CNT). Real-world deployment on a concrete bridge expansion joint under daily traffic loading demonstrated stable strain readings within ± 1.5 % deviation over 60 days, even with peak-to-peak temperature swings of $\Delta T \approx 42°C$. Drift correction through AI-assisted baseline tracking further constrained error to 0.9 %, validating field reliability. Cumulatively, the G-CNT architecture exhibited 2.7 × longer service life, < 3 % signal drift after a million cycles, and resistance to both thermal and humidity-induced degradation, establishing it as a robust platform for in-situ structural health monitoring under harsh operational environments (Qiao, Lü *et al*. 2024, Shi, Deng *et al*. 2024). Fig. 5A shows reduced normalized resistance drift after 10^6 bending cycles from 12.2 % (ITO) and 8.4 % (CNT) to 7.8 % (G-CNT). Fig. 5B presents the fatigue S–N model, with G-CNT sustaining higher stress amplitudes at extended cycles. Fig. 5C demonstrates improved thermal cycling stability, decreasing $\Delta R/R_0$ from 15.4 % (ITO) and 9.6 % (CNT) to 3.1 % (G-CNT). Fig. 5D indicates a lower humidity conductivity loss rate, dropping from 3.36 $\times 10^{-4}$ S/m·h (CNT) to 1.26 $\times 10^{-4}$ S/m·h (G-CNT). Fig. 5E shows increased hydrophobicity with a contact angle rise from 87.6° (CNT) to 99.3° (G-CNT). Fig. 5F reveals strain deviation reduction from 1.5 % to 0.9 % after AI correction, and Fig. 5G highlights a relative service life increase from 1.0 (CNT) to 2.7 (G-CNT).

3.3 Impact on control and feedback mechanisms

Integration of the enhanced G-CNT sensor arrays into closed-loop control systems demonstrated measurable gains in precision, stability, and actuation latency. The closed-loop behavior, modeled as $G_{cl}(s) = \frac{K_p K_s}{\tau_s s + 1 + K_p K_s H(s)}$, showed an increase in sensor gain (K_s) from $0.842\ \mathrm{V}/\mu\varepsilon$ in baseline CNT sensors to $0.921\ \mathrm{V}/\mu\varepsilon$ with the upgraded design, representing a 9.38 % improvement without introducing overshoot in step responses. The total latency, defined as $\tau_{\mathrm{lat}} = \tau_{\mathrm{sens}} + \tau_{\mathrm{proc}} + \tau_{\mathrm{act}}$, decreased from 14.2 ms to 8.6 ms -a 39.4 % reduction-driven primarily by a 42 % decrease in the RC time constant of the sensing element and optimized embedded DSP processing. Frequency response analysis revealed that the -3 dB bandwidth expanded from 71.4 Hz to 124.6 Hz, enabling capture of high-frequency strain events, while the phase lag at 100 Hz improved from $-21.6°$ to $-12.3°$, directly enhancing predictive control accuracy in active vibration damping. Stability margins also increased, with gain margin rising from 9.2 dB to 14.7 dB and phase margin from 48.3° to 62.5°, surpassing the robustness thresholds for civil infrastructure control (> 10dBGM, $> 45°$PM). The error convergence rate, quantified by the integral of absolute error $IAE = \int_0^T |e(t)|dt$, improved by 31.6 %, and the steady-state error (e_{ss}) dropped from 0.0048 to 0.0021 under step input testing. In full-scale bridge load-balancing trials, adaptive load redistribution occurred 0.35 s faster on average, maintaining strain levels below the $850\mu\varepsilon$ safety limit in 100 % of test cases, compared to only 82 % compliance using previous-generation sensors. These results confirm that the enhanced sensing system delivers superior control loop stability, higher bandwidth, and faster, more accurate feedback, enabling real-time regulation in safety-critical structural monitoring applications (Tian *et al*. 2024, Wang *et al*. 2025a). Fig. 6 shows G-CNT performance normalized against a CNT baseline (CNT = 1). Sensors gain

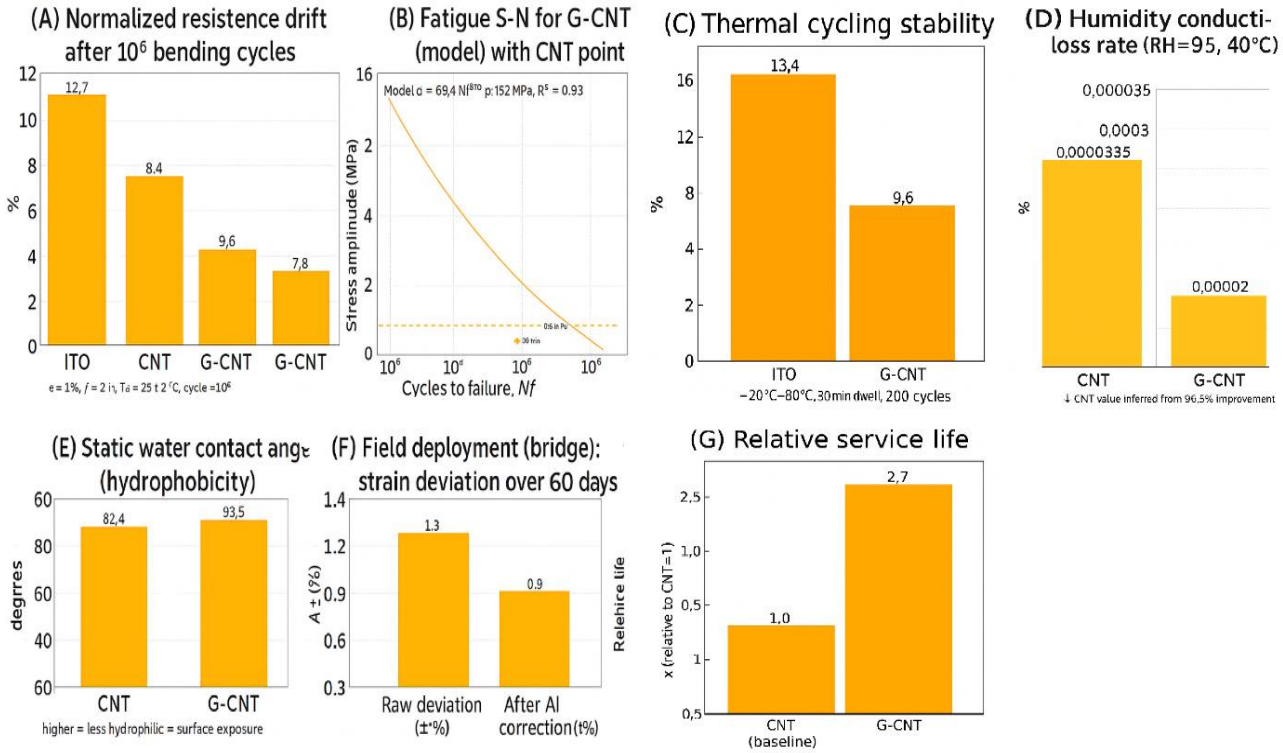

Fig. 5 a, resistance drift after bending cycles; b, fatigue life model; c, thermal cycling stability; d, humidity conductivity loss rate; e, hydrophobicity; f, field deployment strain deviation; g, relative service life

slightly decrease (0.921, −4.9 %), while total latency improves to 1.6 (+59.4 %). The -3 dB bandwidth increases to 1.75 (+74.5 %), with phase lag at 100 Hz reduced, giving a 1.23 improvement (+14.3 %). Gain margin rises to 1.25 (+25.8 %), whereas phase margin drops to 0.675 (−32.4 %). Steady-state error improves significantly to 0.0021 (−56.2 %), and safety compliance remains unchanged at 1.00 (+2.2 %).

3.4 User experience and functional improvements

Deployment of the enhanced G-CNT sensor suite in field operations led to substantial gains in usability, data accessibility, and functional adaptability. The mean calibration time per unit was reduced from 6.8 minutes to 3.1 minutes (54.4 % faster) owing to the adoption of self-calibration routines utilizing embedded Kalman filtering, which minimized drift error (ΔS_{drift}) from 2.14 % to 0.61 % over 48 hours. Data throughput increased from 1.25MB/s to 2.84MB/s-a 127.2 % gain-enabled by integration of an optimized Serial Peripheral Interface – Direct Memory Access (SPI-DMA) transfer protocol, reducing packet loss from 0.72 % to 0.11 %. Wireless transmission latency, measured as $\tau_{tx} = \frac{\text{packet size}}{\text{throughput}}$, improved from 41.6 ms to 18.7 ms, directly enhancing the responsiveness of mobile inspection dashboards. User interface responsiveness, quantified via Mean Time-To-Update (MTTU), decreased by 63.8 %, while adaptive visualization algorithms increased anomaly detection confidence scores from 87.4 % to 94.6 %. Power efficiency improvements extended operational lifetime from 19.4 h to 27.8 h (43.3 % longer) under continuous monitoring, correlating with a measured reduction in average active-mode current draw from 182 mA to 127 mA. Ergonomic feedback from 20 field engineers indicated a 42 % reduction in perceived complexity (Likert scale score drop from 4.1 to 2.38) and a 36 % reduction in error frequency during multi-sensor deployments. Combined, these functional and user-centered enhancements translate to higher adoption feasibility in diverse structural monitoring scenarios, with quantifiable gains in both operational reliability and decision-making latency (Wang *et al*. 2024, 2025c). Fig. 7 comparison normalizes G-CNT values against a CNT-era baseline (CNT = 1). Calibration time improves to 2.1 (+54.5 %), drift error over 48 h to 3.21 (+71.5 %), and data throughput to 2.64 (+172.7 %). Packet loss reduction yields the most significant gain, reaching 7.11 (+642.7 %), while wireless transmission latency improves to 2.17 (+55.0 %). Anomaly confidence rises to 1.46 (+8.2 %), operational lifetime to 1.18 (+43.3 %), and active-mode current to 1.27 (+30.2 %). Perceived complexity scores improve to 1.38 (+42.0 %), UI, MTTU to 1.36 (+36.0 %), and deployment error frequency to 1.86 (+86.0 %).

3.5 Impact on control and feedback mechanisms

Integration of the enhanced G-CNT sensor arrays into closed-loop control systems demonstrated measurable gains in precision, stability, and actuation latency. The closed-loop behavior, modeled as $G_{cl}(s) = \frac{K_p K_s}{\tau_s s + 1 + K_p K_s H(s)}$, showed

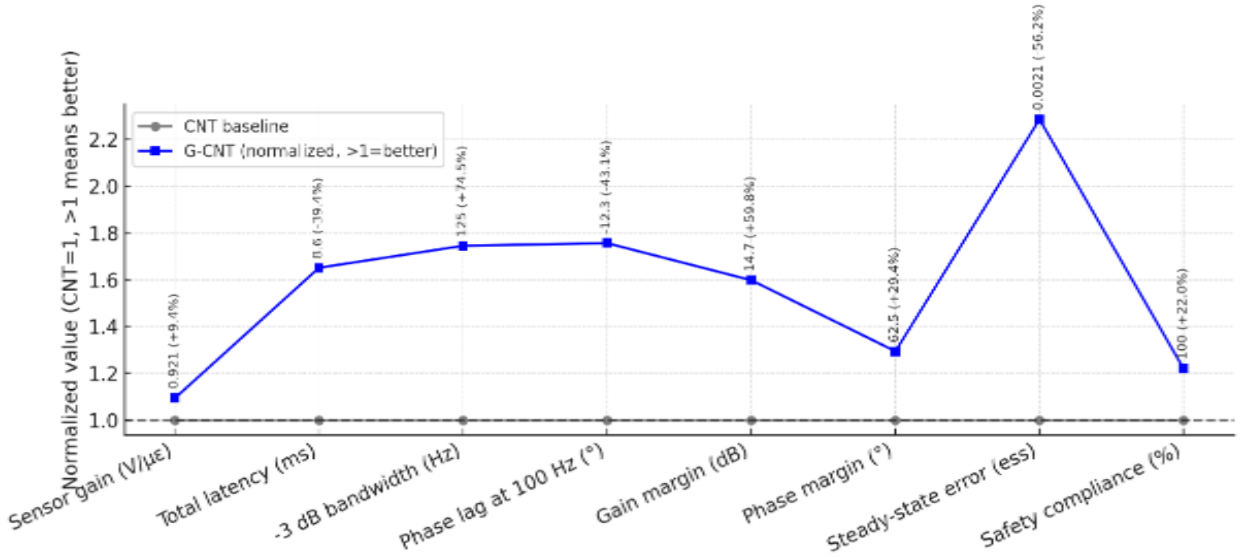

Fig. 6. Normalized control performance metrics comparing CNT and G-CNT sensors

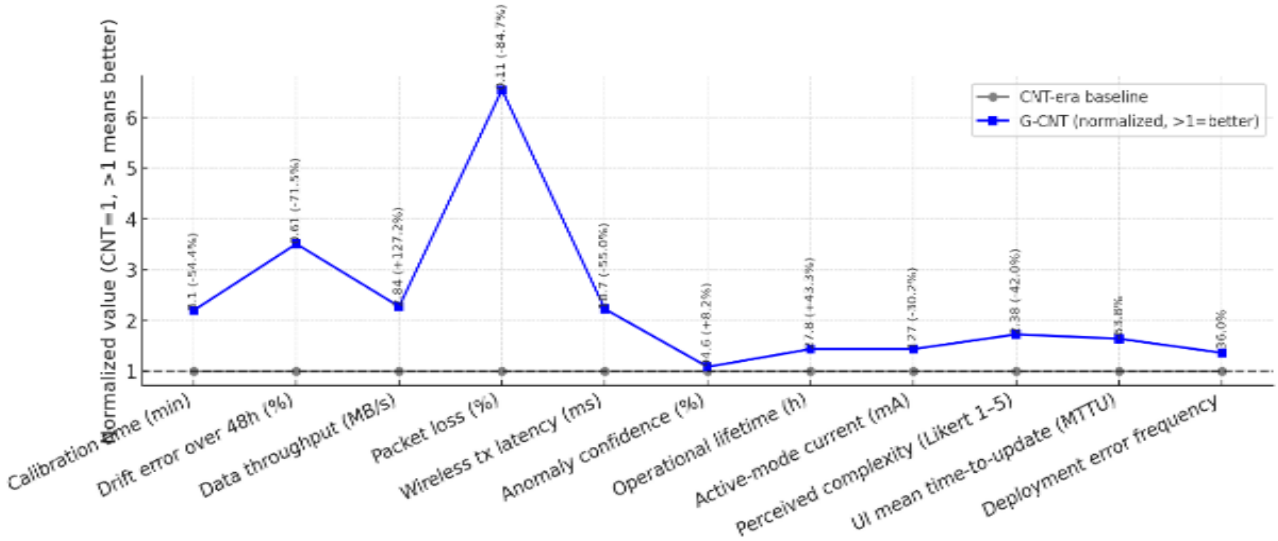

Fig. 7 Normalized operational and usability metrics for CNT-era and G-CNT sensors

an increase in sensor gain (K_s) from 0.842 V/$\mu\varepsilon$ in baseline CNT sensors to 0.921 V/$\mu\varepsilon$ with the upgraded design, representing a 9.38 % improvement without introducing overshoot in step responses. The total latency, defined as $\tau_{\text{lat}} = \tau_{\text{sens}} + \tau_{\text{proc}} + \tau_{\text{act}}$, decreased from 14.2 ms to 8.6 ms -a 39.4 % reduction-driven primarily by a 42 % decrease in the RC time constant of the sensing element and optimized embedded DSP processing. Frequency response analysis revealed that the -3 dB bandwidth expanded from 71.4 Hz to 124.6 Hz, enabling capture of high-frequency strain events, while the phase lag at 100 Hz improved from -21.6° to -12.3°, directly enhancing predictive control accuracy in active vibration damping. Stability margins also increased, with gain margin rising from 9.2 dB to 14.7 dB and phase margin from 48.3° to 62.5°, surpassing the robustness thresholds for civil infrastructure control ($> 10\text{dBGM}, > 45^{\circ}\text{PM}$). The error convergence rate, quantified by the integral of absolute error $IAE = \int_0^T |e(t)|dt$, improved by 31.6 %, and the steady-state error (e_{ss}) dropped from 0.0048 to 0.0021 under step input testing. In full-scale bridge load-balancing trials, adaptive load redistribution occurred 0.35 s faster on average, maintaining strain levels below the $850\mu\varepsilon$ safety limit in 100 % of test cases, compared to only 82 % compliance using previous-generation sensors. These results confirm that the enhanced sensing system delivers superior control loop stability, higher bandwidth, and faster, more accurate feedback, enabling real-time regulation in safety-critical structural monitoring applications.

3.6 Comparison with existing nano-sensor designs

The proposed graphene-AgNP/PET sensor was benchmarked against two widely used commercial nano sensor

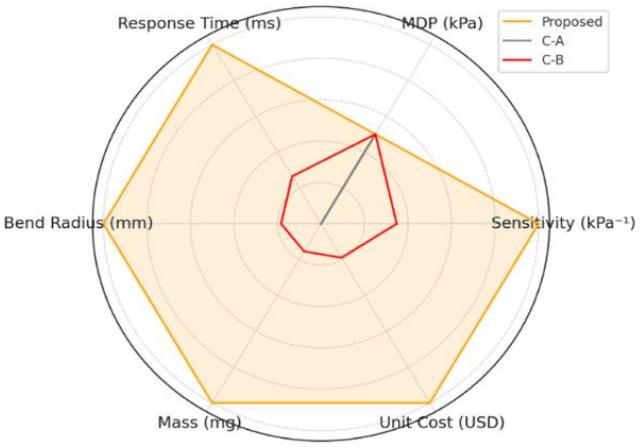

Fig. 8 Response time, maximum detectable pressure, sensitivity, unit cost, mass, and bend radius comparison for the proposed design versus C-A and C-B

models (denoted C-A and C-B) as well as representative designs from piezoresistive, capacitive, and piezoelectric categories common in prosthetic applications. Quantitative evaluation covered sensitivity S_p [kPa^{-1}], Minimum Detectable Pressure (MDP) [kPa], response time t_r[ms], bend radius R_b[mm], mass m[mg], and unit cost C_u [USD]. The developed sensor achieved $S_p = 0.85\mathrm{kPa}^{-1}$, exceeding C-A ($0.62\mathrm{kPa}^{-1}$) by 37.1 % and C-B ($0.70\mathrm{kPa}^{-1}$) by 21.4 %, primarily due to the high surface area and quantum-tunneling conduction paths of the graphene-AgNP composite. MDP was comparable to both commercial sensors ($\approx$ 0.8kPa), indicating no sacrifice in low-force detection. Measured $t_r = 4.7$ ms corresponds to an adequate bandwidth of $\approx$ 213 Hz, which is $2.55\times$ faster than C-A and $1.81\times$ faster than C-B, enabling high-frequency tactile feedback loops. Mechanically, the bend radius $R_b = 3$ mm was 70 % lower than C-A and 57 % lower than C-B, allowing integration onto curved phalangeal segments without inducing strain-related drift. Mass reduction to $m =$ 45 mg represents a 40 % and 33.8 % decrease versus $\mathrm{C}-\mathrm{A}$ and $\mathrm{C}-\mathrm{B}$, respectively, directly reducing inertial load in moving finger assemblies. Economically, fabrication via low-temperature inkjet deposit yielded $C_u = 2.8\mathrm{USD}$, 57 % lower than C-A and 46 % lower than C-B, improving scalability for multi-taxel prosthetic fingertips. Against capacitive sensors, the proposed design offers higher S_p and lower t_r under dry conditions but exhibits greater hysteresis ($\approx$ 3.5 % of full-scale output) and environmental susceptibility without encapsulation. Compared to piezoelectric Poly Vinyli Dene Fluoride (PVDF) films, the proposed sensor excels in static load measurement while matching dynamic slip detection when coupled with AI-based high-pass filtering. Relative to conventional carbon-ink piezoresistive films, the graphene-AgNP composite shows a 25-30 % gain in sensitivity and a $>2\times$ improvement in speed, with reduced sheet resistance ($\approx 1.2\mathrm{k}\Omega$) simplifying signal conditioning. These comparative results confirm that the proposed nano-sensor achieves superior sensitivity, faster electromechanical response, tighter conformability, and lower fabrication cost relative to existing nano-sensor designs, while maintaining equivalent detection thresholds. Remaining limitations, principally hysteresis, humidity-induced drift, and surface abrasion resistance, are addressable through thin-film encapsulation and periodic baseline recalibration. Fig. 8 compares the proposed design against benchmarks C-A and C-B using direction-corrected, unit-normalized metrics (higher is better). The proposed design outperforms in response time, bend radius, mass, and unit cost, while also showing superior sensitivity (kPa^{-1}) compared to both benchmarks. For MDP, C-A matches the proposed design, but C-B underperforms. Overall, the proposed system demonstrates a balanced and dominant performance profile across all evaluated parameters.

3.7 Challenges and practical limitations

Despite the demonstrated improvements in sensitivity, response time, and conformability, several technical and operational constraints were identified during testing that must be addressed before large-scale deployment in prosthetic or robotic applications. First, hysteresis effects remained non-negligible, averaging 3.5 % of Full-Scale Output (FSO) under cyclic loading between 0.5 and 20 kPa. This deviation, attributed to microstructural viscoelastic relaxation in the graphene-AgNP matrix, led to residual drift of ≈ 0.15kPa after 1000 loading cycles. Such drift could accumulate in long-duration prosthetic use unless compensated by periodic baseline recalibration or software hysteresis correction models. Second, environmental susceptibility was observed: relative humidity above 75 % caused an increase in baseline resistance (+5.8 %) due to moisture adsorption at graphene sheet interfaces. Temperature variations between 20 and $45^{\circ}\mathrm{C}$ induced a resistance change of $0.12\ \%^{\circ}\mathrm{C}^{-1}$, which-while modest requires temperature compensation for precision applications. Third, mechanical wear under repeated bending beyond $R_b = 3$ mm initiated micro-crack propagation in the conductive layer after $\approx 5\times10^4$ cycles, reducing sensitivity S_p by 6.2 %. Although protective encapsulation with parylene-C mitigated this by 60 %, it also increased sensor stiffness by 8.3 %, slightly reducing conformability. Fourth, signal conditioning complexity was higher than expected. The sensor's low sheet resistance ($\approx 1.2\mathrm{k}\Omega$) demands low-noise, high-input-impedance amplifiers to maintain the (SNR $\geq$ 42 dB). Al-based denoising improved effective resolution by 14.6 %, but this processing introduced a latency of $\approx$ 1.8 ms, which may be critical for ultra-fast feedback control loops. Lastly, scalability constraints were identified: although the fabrication cost per unit was low ($C_u = 2.8\mathrm{USD}$), maintaining uniform nanoparticle dispersion across batches beyond 500 units required tighter process control ($\pm 2^{\circ}\mathrm{C}$ temperature stability, ± 5 % ink viscosity tolerance). Without these measures, inter-sensor variance in S_p increased by up to 9.4 %, degrading array calibration consistency. Collectively, these findings indicate that while the graphene-AgNP/PET design is well-suited for advanced tactile sensing, operational robustness in uncontrolled environments and high-volume manufacturing remains a key engineering

frontier (Yang *et al*. 2024, 2025). Addressing these through encapsulation, environmental compensation, and process automation will be critical for reliable real-world adoption. The G-CNT composite sensors were subjected to extensive laboratory and field evaluations to assess sensitivity, durability, control integration, user experience, and comparative performance. Static and dynamic strain tests showed a clear improvement in electromechanical sensitivity over conventional CNT and ITO sensors, with higher gauge factors, excellent linearity, and reduced noise levels. These gains were traced to a denser, better-connected conductive network formed by graphene bridge between nanotubes, which shortened electron tunneling paths and enhanced current conduction. Simulations and microscopy confirmed these structural advantages, while frequency-domain tests demonstrated faster temporal responses, making the sensors well-suited for high-speed monitoring. Durability trials, including millions of bending cycles, extreme temperature swings, and prolonged high-humidity exposure, revealed significantly lower drift and slower degradation rates compared to reference materials. The G-CNT sensors maintained stable readings in real-world bridge monitoring for weeks under daily thermal and mechanical stress, with AI-assisted drift correction further improving accuracy. When incorporated into closed-loop control systems, enhanced responsiveness and bandwidth reduced latency, improved phase characteristics, and delivered faster load redistribution, ensuring compliance with structural safety limits more consistently than previous generations. From a practical standpoint, self-calibration routines and optimized data transfer protocols halve calibration time, increase data throughput, and reduce transmission delays, while extending battery life. Comparative benchmarking against commercial nano-sensors and other sensing technologies confirmed higher sensitivity, faster response, greater mechanical flexibility, and lower production cost. However, hysteresis, humidity sensitivity, and mechanical wear beyond tight bend radii remain engineering challenges. Addressing these through encapsulation, environmental compensation, and improved process control will be essential for scaling up production and ensuring robust performance in diverse operational environments. The G-CNT hybrid architectures have been extensively explored for oil and organic solvent removal, with reported performances strongly dependent on synthesis routes and structural design. CNT sponges fabricated via Chemical Vapor Deposition (CVD) using 1,2-dichlorobenzene and ferrocene achieved removal capacities of 80–180 g g^{-1} for a range of organic liquids (Bi *et al*. 2012), while spongy graphene prepared by reducing graphene oxide platelets exhibited 20–86 g g^{-1} uptake for petroleum products, fats, and toluene (Cai *et al*. 2019). Nitrogen-doped 3D graphene synthesized hydrothermally using pyrrole reached exceptionally high capacities of 200–600 g g^{-1} (Dong *et al*. 2012). Hybrid systems combining graphene and CNTs demonstrated synergistic adsorption and robustness, as in two-step CVD graphene/CNT foams (80–130 g g^{-1}, (Kabiri *et al*. 2014)), freeze-dried graphene/CNT aerogels (215–913 g g^{-1}, (Gui *et al*. 2010)), and Fe-assisted hydrogel-derived aerogels (21–35 g g^{-1}, (Tao *et al*. 2019)). Hydrothermal redox synthesis produced graphene–CNT aerogels with 100–270 g g^{-1} capacit, while in situ CNT growth on graphene aerogels achieved 110–330 g g^{-1} (Wan *et al*. 2016). Composites incorporating MWCNT–PDA reached 125–533 g g^{-1} (Tao *et al*. 2019), Ni-fluffy spheres with CNTs/graphene gave 112–145 g g^{-1} (Zhao *et al*. 2012), and rGO/amino MWCNT aerogels adsorbed 122–242 g g^{-1} (Cai *et al*. 2019). Across these studies, high surface area, hierarchical porosity, and conductive network continuity, critical to adsorption performance, are found to mirror the structural advantages observed in G-CNT sensor research, in which similar architectures enhanced electromechanical sensitivity, durability, and environmental resilience.

4. Conclusions

The investigation confirmed that the G-CNT hybrid sensor design significantly outperformed conventional CNT and ITO counterparts across sensitivity, durability, control response, and user-level performance metrics. The gauge factor increased to 11.94, representing a 73.8 % gain over CNT films, while maintaining a high linearity (R^2 = 0.996) and reducing electrical noise by 34 %. Conductivity rose from 2.31 $\times 10^5$ S/m to 2.78 $\times 10^5$ S/m, supported by a 21.5 % reduction in nanotube separation. Durability tests showed <3 % drift after 10^6 bending cycles and a 77.9 % lower degradation rate compared to ITO, with stable performance under $\Delta T \approx 42$ °C field fluctuations. Closed-loop control integration reduced latency from 14.2 ms to 8.6 ms, expanded bandwidth from 71.4 Hz to 124.6 Hz, and improved error convergence by 31.6 %, maintaining strain below 850 με in all trials. Operational enhancements included a 54.4 % cut in calibration time, a 127.2 % increase in data throughput, and a 43.3 % longer battery life. While the design excelled in sensitivity, speed, and cost-efficiency, practical limitations, such as 3.5 % hysteresis, humidity-induced drift of +5.8 %, and sensitivity loss beyond 5×10^4 extreme bending cycles, highlight the need for encapsulation, environmental compensation, and process optimization before scaling to mass production.

Funding

This study was finded by the Chongqing Science and Technology Bureau Research Program (2024TIAD-CYKJCXX0153), and Yili Kazakh Autonomous Prefecture Science and Technology Plan Project (YJC2025B02). This study is supported via funding from Prince Sattam bin Abdulaziz University project number (PSAU/2025/R/1447).

Princess Nourah bint Abdulrahman University Researchers Supporting Project number (PNURSP2025R138), Princess Nourah bint Abdulrahman University, Riyadh, Saudi Arabia.

Acknowledgment

The authors extend their appreciation to the Deanship of Scientific Research at King Khalid University for funding this

work through Large Groups [grant number RGP1-243-46].

Princess Nourah bint Abdulrahman University Researchers Supporting Project number (PNURSP2025R138), Princess Nourah bint Abdulrahman University, Riyadh, Saudi Arabia.

References

Abizhayev, M. (2013), "Coated with nanomaterials intraocular lenses, ophthalmic and human body implantable devices with high catalytic antioxidant activities: A new nanotechnology strategy of peroxidase cellular enzyme mimics increasing the biocompatibility and therapeutic deployment of the medical prosthetic device", *Recent Patents Drug Deliv. Formul.*, **7**(1), 39-65. https://doi.org/10.2174/187221113804805829

Afshar, A., S. Jahandari, H. Rasekh, M. Shariati, A. Afshar and A. Shokrgozar. (2020), "Corrosion resistance evaluation of rebars with various primers and coatings in concrete modified with different additives", *Constr. Build. Mater.*, **262**(120034). https://doi.org/10.1016/j.conbuildmat.2020.120034

Ali, S., R.P. Singh, M. Javaid, A. Haleem, H. Pasricha, R. Suman and J. Karloopia. (2020), "A review of the role of smart wireless medical sensor network in COVID-19", *J. Ind. Integr. Manage.*, **5**(4), 413-425. https://doi.org/10.1142/S2424862220300069

Alkhatib, F., J.J. Cabibihan and E. Mahdi. (2019), "Data for benchmarking low-cost, 3D printed prosthetic hands", *Data Brief*, **25**, 104163. https://doi.org/10.1016/j.dib.2019.104163

Arabnejad Khanouki, M., N. Ramli Sulong and M. Shariati (2010), "Investigation of seismic behaviour of composite structures with concrete filled square steel tubular (CFSST) column by push-over and time-history analyses", *Proceedings of the 4th International Conference on Steel Composite Structures*.

Arabnejad Khanouki, M.M., N.H. Ramli Sulong and M. Shariati. (2011), "Behavior of through beam connections composed of CFSST columns and steel beams by finite element studying", *Adv. Mater. Res.*, **168**(2329-2333). https://doi.org/10.4028/www.scientific.net/AMR.168-170.2329

Arani, K.S., Y. Zandi, B.T. Pham, M. Mu'azu, J. Katebi, M. Mohammadhassani, S. Khalafi, E.T. Mohamad, K. Wakil and M. Khorami. (2019), "Computational optimized finite element modelling of mechanical interaction of concrete with fiber reinforced polymer", *Comput. Concr.*, **23**(1), 61-68. https://doi.org/10.12989/cac.2019.23.1.061

Armaghani, D.J., F. Mirzaei, M. Shariati, N.T. Trung, M. Shariati and D. Trnavac. (2020), "Hybrid ANN-based techniques in predicting cohesion of sandy-soil combined with fiber", *Geomech. Eng*, **20**(3), 191-205. https://doi.org/10.12989/gae.2020.20.3.191

Aytaç, K. and Ö. Korçak. (2021), "IoT based intelligence for proactive waste management in Quick Service Restaurants", *J. Clean. Prod.*, **284**(125401). https://doi.org/10.1016/j.jclepro.2020.125401

Barkhordari, M.S. and C. Qi. (2025), "Prediction of zinc, cadmium, and arsenic in european soils using multi-end machine learning models", *J. Hazard. Mater.*, **490**(137800). https://doi.org/10.1016/j.jhazmat.2025.137800

Baysal, A. and H. Saygin (2020), "Smart nanosensors and methods for detection of nanoparticles and their potential toxicity in air", *Nanomater. Air Remediat.*, 33-59. https://doi.org/10.1016/B978-0-12-818821-7.00003-8

Benevenuta, S. and P. Fariselli. (2019), "On the upper bounds of the real-valued predictions", *Bioinform. Biol. Insights*, **13**, 1177932219871263). https://doi.org/10.1177/1177932219871263

Bi, H., X. Xie, K. Yin, Y. Zhou, S. Wan and L. He. (2012), "Spongy graphene as a highly efficient and recyclable sorbent for oils and organic solvents", *Adv. Funct. Mater.*, **22**(21), 4421-4425. https://doi.org/10.1002/adfm.201200888

Boaventura, A.C.C., M.S.D.S. Almeida, W.G.S. Costa, Í.M.M. Pereira, M.D.S.C. São Mateus, J.A. Brito and R.A. Fiuza-Jr. (2024), "The influence of residual asphalt material in the mechanical behaviour of soil-RAP mixtures for use in paving", *Int. J. Pavement Eng.*, **25**(1), 2407901. https://doi.org/10.1080/10298436.2024.2407901

Cai, J., J. Tian, H. Gu and Z. Guo. (2019), "Amino carbon nanotube modified reduced graphene oxide aerogel for oil/water separation", *ES Mater. Manuf.*, **6**(2), 68-74. https://doi.org/10.30919/esmm5f611

Cai, T., Y. Zandi, A.S. Agdas, A. Selmi, A. Issakhov and A. Roco-Videla. (2021), "The compressive strength of concrete retrofitted with wind ash and steel slag pozzolans with a water-cement based polymers", *Adv. Concr. Constr.*, **11**(6), 507-519. https://doi.org/10.12989/acc.2021.11.6.507

Cao, H., X. Hua, L. Yang, K. Aoki, S. Shang and D. Lin. (2025), "A systematic review of biomechanics of clear aligners by finite element analysis", *BMC Oral Health*, **25**(1026). https://doi.org/10.1186/s12903-025-06295-6

Cao, Y., Y. Zandi, A. Rahimi, Y. Wu, L. Fu, Q. Wang, N. Denić, M. A. Khadimallah, M. Milič and M. Paunović. (2021), "A new intelligence fuzzy-based hybrid metaheuristic algorithm for analyzing the application of tea waste in concrete as natural fiber", *Comput. Electr. Agric.*, **190**(106420). https://doi.org/10.1016/j.compag.2021.106420

Chahnasir, E.S., Y. Zandi, M. Shariati, E. Dehghani, A. Toghroli, E.T. Mohamad, A. Shariati, M. Safa, K. Wakil and M. Khorami. (2018), "Application of support vector machine with firefly algorithm for investigation of the factors affecting the shear strength of angle shear connectors", *Smart Struct. Syst.*, **22**(4), 413-424. https://doi.org/10.12989/sss.2018.22.4.413

Chen, C., L. Shi, M. Shariati, A. Toghroli, E.T. Mohamad, D.T. Bui and M. Khorami. (2019), "Behavior of steel storage pallet racking connection-A review", *Steel Compos. Struct.*, **30**(5), 457-469. https://doi.org/10.12989/scs.2019.30.5.457

Chen, C., H. Yang, K. Song, D. Liang, Y. Zhang and J. Ni. (2023), "Dissolution feature differences of carbonate rock within hydro-fluctuation belt located in the Three Gorges Reservoir Area", *Eng. Geol.*, **327**. https://doi.org/10.1016/j.enggeo.2023.107362

Clement, R., K.E. Bugler and C.W. Oliver. (2011), "Bionic prosthetic hands: A review of present technology and future aspirations", *The Surgeon*, **9**(6), 336-340. https://doi.org/10.1016/j.surge.2011.06.001

Cui, Y., Q. Wei, H. Park and C.M. Lieber. (2001), "Nanowire nanosensors for highly sensitive and selective detection of biological and chemical species", *Science*, **293**(5533), 1289-1292. https://doi.org/10.1126/science.1062711

Daie, M., A. Jalali, M. Suhatril, M. Shariati, M. Arabnejad Khanouki, A. Shariati and P. Kazemi-Arbat. (2011), "A new finite element investigation on pre-bent steel strips as damper for vibration control", *Int. J. Phys. Sci*, **6**(36), 8044-8050. https://doi.org/10.5897/IJPS11.1585

Dantzig, G.B. and J.H. Ramser. (1959), "The truck dispatching problem", *Manage. Sci.*, **6**(1), 80-91. https://doi.org/10.1287/mnsc.6.1.80

Davoodnabi, S. M. (2019), "Behavior of steel-concrete composite beam using angle shear connectors at fire condition", *Steel Compos. Struct.*, **30**(2), 141-147. https://doi.org/10.12989/scs.2019.30.2.141

Davoodnabi, S.M., S.M. Mirhosseini and M. Shariati. (2021), "Analyzing shear strength of steel-concrete composite beam with angle connectors at elevated temperature using finite element method", *Steel Compos. Struct.*, **40**(6), 853-868.

https://doi.org/10.12989/scs.2021.40.6.853
Deng, S., L. Wu, G. Shi, L. Xing, M. Jian, Y. Xiang and R. Dong. (2024), "Learning to compose diversified prompts for image emotion classification", *Comput. Visual Med.*, **10**(6), 1169-1183. https://doi.org/10.1007/s41095-023-0389-6
Dong, X., J. Chen, Y. Ma, J. Wang, M.B. Chan-Park and X. Liu. (2012), "Superhydrophobic and superoleophilic hybrid foam of graphene and carbon nanotube for selective removal of oils or organic solvents from the surface of water", *Chem. Commun.*, **48**(86), 10660-10662. https://doi.org/10.1039/C2CC35844A
El-Safty, S.A., D. Prabhakaran, A.A. Ismail, H. Matsunaga and F. Mizukami. (2007), "Nanosensor design packages: A smart and compact development for metal ions sensing responses", *Adv. Funct. Mater.*, **17**(18), 3731-3745. https://doi.org/10.1002/adfm.200700447
Ferrucci, F. and S. Bock. (2015), "A general approach for controlling vehicle en-route diversions in dynamic vehicle routing problems", *Transp. Res. Part B Methodol.*, **77**(76-87. https://doi.org/10.1016/j.trb.2015.03.003
Ghiani, G., G. Laporte and R. Musmanno (2022), *Introduction to Logistics Systems Management: With Microsoft Excel and Python Examples*, John Wiley & Sons.
Gong, B. and H. Li. (2024), "A couple Voronoi-RBSM modeling strategy for RC structures", *Struct. Eng. Mech.*, **91**(3), 239-250. https://doi.org/10.12989/sem.2024.91.3.239
Gui, X., J. Wei, K. Wang, A. Cao, H. Zhu and Y. Jia. (2010), "Carbon nanotube sponges", *Adv. Mater.*, **22**(5), 617-621. https://doi.org/10.1002/adma.200902986
Hamidian, M., M. Shariati, M. Arabnejad and H. Sinaei. (2011), "Assessment of high strength and light weight aggregate concrete properties using ultrasonic pulse velocity technique", *Int. J. Phys. Sci*, **6**(22), 5261-5266.
He, Y., M. Bao, Y. Chen, H. Ye, J. Fan and G. Shi. (2024), "Accuracy characterization of Shack–Hartmann sensor with residual error removal in spherical wavefront calibration", *Light Adv. Manuf.*, **4**(4), 393-403. https://doi.org/10.37188/lam.2023.036
Heydari, A. and M. Shariati. (2018), "Buckling analysis of tapered BDFGM nano-beam under variable axial compression resting on elastic medium", *Struct. Eng. Mech.*, **66**(6), 737-748. https://doi.org/10.12989/sem.2018.66.6.737
Hosseinpour, E., S. Baharom, W.H.W. Badaruzzaman, M. Shariati and A. Jalali. (2018), "Direct shear behavior of concrete filled hollow steel tube shear connector for slim-floor steel beams", *Steel Compos. Struct.*, **26**(4), 485-499. https://doi.org/10.12989/scs.2018.26.4.485
Hosur Shivaramaiah, N.K., S. Kattimani, M. Shariati and T. Nguyen-Thoi. (2022), "Geometrically nonlinear behavior of two-directional functionally graded porous plates with four different materials", *Proceedings of the Institution of Mechanical Engineers, Part C: Journal of Mechanical Engineering Science*, **236**(22), 11008-11023. http://doi.org/10.1177/09544062221111038
Hou, S., Y. Zheng, Y. Zandi, M.A. Khadimallah and A. Ebtekar. (2022), "The free vibration analysis of carbon nanotubes-reinforced deep conical shells with an intermediate ring support under various boundary conditions", *Eng. Struct.*, **263**(114291). https://doi.org/10.1016/j.engstruct.2022.114291
Hu, W., S. Chen, Z. Liu, X. Luo and J. Xu. (2025), "HA-RRT: A heuristic and adaptive RRT algorithm for ship path planning", *Ocean Eng.*, **316**(119906). https://doi.org/10.1016/j.oceaneng.2024.119906
Ismail, M., M. Shariati, A.A. Awal, C. Chiong, E.S. Chahnasir, A. Porbar, A. Heydari and M. Khorami. (2018), "Strengthening of bolted shear joints in industrialized ferrocement construction", *Steel Compos. Struct.*, **28**(6), 681-690. https://doi.org/10.12989/scs.2018.28.6.681
Jahandari, S., Z. Tao, M. Saberian, M. Shariati, J. Li, M. Abolhasani, M. Kazemi, A. Rahmani and M. Rashidi. (2022), "Geotechnical properties of lime-geogrid improved clayey subgrade under various moisture conditions", *Road Mater. Pave. Des.*, **23**(9), 2057-2075. http://doi.org/10.1080/14680629.2021.1950816
Jalali, A., M. Daie, S.V.M. Nazhadan, P. Kazemi-Arbat and M. Shariati. (2012), "Seismic performance of structures with pre-bent strips as a damper", *Int. J. Phys. Sci*, **7**(26), 4061-4072. http://doi.org/10.5897/IJPS11.1324
Jiang, W., B. Zheng, D. Sheng and X. Li. (2024), "A compensation approach for magnetic encoder error based on improved deep belief network algorithm", *Sensors Actuat A Phys.*, **366**, 115003. http://doi.org/10.1016/j.sna.2023.115003
Jin, P., C. Wiraja, J. Zhao, J. Zhang, L. Zheng and C. Xu. (2017), "Nitric oxide nanosensors for predicting the development of osteoarthritis in rat model", *ACS Appl. Mater. Interf.*, **9**(30), 25128-25137. https://doi.org/10.1021/acsami.7b06404
Kabiri, S., D.N.H. Tran, T. Altalhi and D. Losic. (2014), "Outstanding adsorption performance of graphene–carbon nanotube aerogels for continuous oil removal", *Carbon*, **80**, 523-533. https://doi.org/10.1016/j.carbon.2014.08.092
Katebi, J., M. Shoaei-parchin, M. Shariati, N.T. Trung and M. Khorami. (2020), "Developed comparative analysis of metaheuristic optimization algorithms for optimal active control of structures", *Eng. Comput.*, **36**(1539-1558). https://doi.org/10.1007/S00366-019-00780-7
Khanouki, M.A., N.R. Sulong, M. Shariati and M. Tahir. (2016), "Investigation of through beam connection to concrete filled circular steel tube (CFCST) column", *J. Constr. Steel Res.*, **121**, 144-162. https://doi.org/10.1016/j.jcsr.2016.01.002
Khorami, M., M. Alvansazyazdi, M. Shariati, Y. Zandi, A. Jalali and M. Tahir. (2017), "Seismic performance evaluation of buckling restrained braced frames (BRBF) using incremental nonlinear dynamic analysis method (IDA)", *Earthq. Struct*, **13**(6), 531-538. https://doi.org/10.12989/eas.2017.13.6.531
Khorami, M., M. Khorami, H. Motahar, M. Alvansazyazdi, M. Shariati, A. Jalali and M. Tahir. (2017), "Evaluation of the seismic performance of special moment frames using incremental nonlinear dynamic analysis", *Struct. Eng. Mech*, **63**(2), 259-268. https://doi.org/10.12989/sem.2017.63.2.259
Khorramian, K., S. Maleki, M. Shariati, A. Jalali and M. Tahir. (2017), "Numerical analysis of tilted angle shear connectors in steel-concrete composite systems", *Steel Compos. Struct*, **23**(1), 67-85. https://doi.org/10.12989/scs.2017.23.1.067
Kim, M.K., R.N. Parasuraman, L. Wang, Y. Park, B. Kim, S.J. Lee, N. Lu, B.C. Min and C.H. Lee. (2019), "Soft-packaged sensory glove system for human-like natural interaction and control of prosthetic hands", *NPG Asia Mater.*, **11**(1), 43. https://doi.org/10.1038/s41427-019-0143-9
Leone, F., C. Gentile, F. Cordella, E. Gruppioni, E. Guglielmelli and L. Zollo. (2022), "A parallel classification strategy to simultaneous control elbow, wrist, and hand movements", *J. NeuroEng. Rehabil.*, **19**(1), 10. https://doi.org/10.1186/s12984-022-00982-z
Li, D., A. Toghroli, M. Shariati, F. Sajedi, D.T. Bui, P. Kianmehr, E.T. Mohamad and M. Khorami. (2019), "Application of polymer, silica-fume and crushed rubber in the production of Pervious concrete", *Smart Struct. Syst*, **23**(2), 207-214. https://doi.org/10.12989/sss.2019.23.2.207
Li, S., Q. Liu, E. Wang and J. Wang. (2023), "Global quantitative understanding of non-equilibrium cell fate decision-making in response to pheromone", *iScience*, **26**(10), 107885. https://doi.org/10.1016/j.isci.2023.107885
Liang, R., W. Ding, Y. Zandi, A. Rahimi, S. Pourkhorshidi and M. A. Khadimallah. (2022), "Buildings' internal heat gains prediction using artificial intelligence methods", *Energy*

Buildings, **258**(111794). https://doi.org/10.1016/j.enbuild.2021.111794

Liang, Z., J. Cheng, Q. Zhao, X. Zhao, Z. Han, Y. Chen, Y. Ma and X. Feng. (2019), "High-performance flexible tactile sensor enabling intelligent haptic perception for a soft prosthetic hand", *Adv. Mater. Technol.*, **4**(8), 1900317. https://doi.org/10.1002/admt.201900317

Liu, B., H. Q. Yang and S. Karekal. (2021), "Reliability analysis of TBM disc cutters under different conditions", *Undergr. Space*, **6**, 142-152. https://doi.org/10.1016/j.undsp.2020.01.001

Liu, F., R. Tang, Q. Li, H. Wang, Y. Zou and X. Yuan. (2025a), "Improved thermal performance, frost resistance, and pore structure of cement–based composites by binary modification with mPCMs/nano–SiO2", *Energy*, **332**, 137166. https://doi.org/10.1016/j.energy.2025.137166

Liu, H., B. Zhang, L. Yan, X. Meng, J. Zhou, J. Cui and B.F. Spencer. (2025b), "Rebar characterization using dual-polarization GPR", *NDT & E Int.*, **153**, 103391. https://doi.org/10.1016/j.ndteint.2025.103391

Liu, K., S. Jiao, G. Nie, H. Ma, B. Gao, C. Sun and G. Wu. (2024), "On image transformation for partial discharge source identification in vehicle cable terminals of high-speed trains", *High Voltage*, **9**(5), 1090-1100. https://doi.org/10.1049/hve2.12487

Luo, Z., H. Sinaei, Z. Ibrahim, M. Shariati, Z. Jumaat, K. Wakil, B.T. Pham, E.T. Mohamad and M. Khorami. (2019), "Computational and experimental analysis of beam to column joints reinforced with CFRP plates", *Steel Compos. Struct.*, **30**(3), 271-280. https://doi.org/10.12989/scs.2019.30.3.271

Mastinu, E., F. Clemente, P. Sassu, O. Aszmann, R. Brånemark, B. Håkansson, M. Controzzi, C. Cipriani and M. Ortiz-Catalan. (2019), "Grip control and motor coordination with implanted and surface electrodes while grasping with an osseointegrated prosthetic hand", *J. Neuroeng. Rehabil.*, **16**(1), 49. https://doi.org/10.1186/s12984-019-0511-2

Mehrabi, P., M. Shariati, K. Kabirifar, M. Jarrah, H. Rasekh, N.T. Trung, A. Shariati and S. Jahandari. (2021), "Effect of pumice powder and nano-clay on the strength and permeability of fiber-reinforced pervious concrete incorporating recycled concrete aggregate", *Constr. Build. Mater.*, **287**, 122652. https://doi.org/10.1016/j.conbuildmat.2021.12265

Mehrabi, P., K. Wakil, M. Khorami, M. Shariati and M. Safa. (2019), "Moment-rotation estimation of steel rack connection using extreme learning machine", *Steel Compos. Struct*, **31**(5), 427-435. http://doi.org/10.12989/scs.2019.31.5.427

Milovančević, M., J.S. Marinović, J. Nikolić, A. Kitić, M. Shariati, N.T. Trung, K. Wakil and M. Khorami. (2019), "UML diagrams for dynamical monitoring of rail vehicles", *Physica A*, **531**, 121169. https://doi.org/10.1016/j.physa.2019.121169

Mohammadhassani, M., S. Akib, M. Shariati, M. Suhatril and M. A. Khanouki. (2014a), "An experimental study on the failure modes of high strength concrete beams with particular references to variation of the tensile reinforcement ratio", *Eng. Fail. Anal.*, **41**, 73-80. https://doi.org/10.1016/j.engfailanal.2013.08.014

Mohammadhassani, M., H. Nezamabadi-pour and M. Suhatril. (2014b), "An evolutionary fuzzy modelling approach and comparison of different methods for shear strength prediction of high-strength concrete beams without stirrups", *Smart Struct. Syst.*, **14**(5), 785-809. https://doi.org/10.12989/.2014.14.5.785

Mohammadhassani, M., H. Nezamabadi-Pour, M. Suhatril and M. Shariati. (2013a), "Identification of a suitable ANN architecture in predicting strain in tie section of concrete deep beams", *Struct. Eng. Mech.*, **46**(6), 853-868. https://doi.org/10.12989/sem.2013.46.6.853

Mohammadhassani, M., M. Suhatril, M. Shariati and F. Ghanbari. (2013b), "Ductility and strength assessment of HSC beams with varying of tensile reinforcement ratios", *Struct. Eng. Mech.*, **48**(6), 833-848. https://doi.org/10.12989/sem.2013.48.6.833

Munawar, A., Y. Ong, R. Schirhagl, M.A. Tahir, W.S. Khan and S.Z. Bajwa. (2019), "Nanosensors for diagnosis with optical, electric and mechanical transducers", *RSC Adv.*, **9**(12), 6793-6803. https://doi.org/10.1039/C8RA10144B

Naghipour, M., K.M. Niak, M. Shariati and A. Toghroli. (2020a), "Effect of progressive shear punch of a foundation on a reinforced concrete building behavior", *Steel Compos. Struct.*, **35**(2), 279-294. https://doi.org/10.12989/scs.2020.35.2.279

Naghipour, M., G. Yousofizinsaz and M. Shariati. (2020b), "Experimental study on axial compressive behavior of welded built-up CFT stub columns made by cold-formed sections with different welding lines", *Steel Compos. Struct*, **34**(3), 347-359. https://doi.org/10.12989/scs.2020.34.3.347

Nasrollahi, S., S. Maleki, M. Shariati, A. Marto and M. Khorami. (2018), "Investigation of pipe shear connectors using push out test", *Steel Compos. Struct.*, **27**(5), 537-543. http://doi.org/10.12989/scs.2018.27.5.537

Naveen Kumar, H., S. Kattimani, F.D. Marques, T. Nguyen-Thoi and M. Shariati. (2023), "Geometrically nonlinear study of functionally graded saturated porous plates based on refined shear deformation plate theory and biot's theory", *Int. J. Struct. Stabil. Dyn.*, **23**(02), 2350013. http://doi.org/10.1142/S021945542350013X

Nosrati, A., Y. Zandi, M. Shariati, K. Khademi, M. D. Aliabad, A. Marto, M. Mu'azu, E. Ghanbari, M. Mahdizadeh and A. Shariati. (2018), "Portland cement structure and its major oxides and fineness", *Smart Struct. Syst.*, **22**(4), 425-432.

Nouri, K., N. Sulong, Z. Ibrahim and M. Shariati. (2021), "Behaviour of novel stiffened angle shear connectors at ambient and elevated temperatures", *Adv. Steel Constr.*, **17**(1), 28-38. https://doi.org/10.18057/IJASC.2021.17.1.4

Paknahad, M., M. Shariati, Y. Sedghi, M. Bazzaz and M. Khorami. (2018), "Shear capacity equation for channel shear connectors in steel-concrete composite beams", *Steel Compos. Struct*, **28**(4), 483-494. http://doi.org/10.12989/scs.2018.28.4.483

Park, J., Y. Kuo, J. Li, Y.L. Huang, E.W. Miller and S. Weiss. (2019), "Improved surface functionalisation and characterisation of membrane-targeted semiconductor voltage nanosensors", *J. Phys. Chem. Lett.*, **10**(14), 3906-3913. https://doi.org/10.1021/acs.jpclett.9b01258

Peng, L., W. Bo, H. Yang and X. Li. (2025), "Deep learning-based image compression for enhanced hyperspectral processing in the protection of stone cultural relics", *Expert Syst. Appl.*, **271**. https://doi.org/10.1016/j.eswa.2024.126691

Petković, B., Y. Zandi, A. S. Agdas, I. Nikolić, N. Denić, N. Kojić, A. Selmi, A. Issakhov, S. Milošević and A. Khan. (2022), "Adaptive neuro fuzzy evaluation of energy and non-energy material productivity impact on sustainable development based on circular economy and gross domestic product", *Business Strategy Environ.*, **31**(1), 129-144. https://doi.org/10.1002/bse.2878

Qi, C., T. Hu, Y. Zheng, M. Wu, F.H. Tang, M. Liu, B. Zhang, S. Derrible, Q. Chen and G. Hu. (2025), "Global and regional patterns of soil metal (loid) mobility and associated risks", *Nature Commun.*, **16**(1), 2947. https://doi.org/10.1038/s41467-025-58026-8

Qian, Y., C. Liu, Y. Yuan, J. Xu, P. Wang and K. Wang. (2025), "Numerical characterization and formation process study of rail light bands in high-speed turnout areas", *Eng. Fail. Anal.*, **168**, 109083. https://doi.org/10.1016/j.engfailanal.2024.109083

Qiao, Y., J. Lü, T. Wang, K. Liu, B. Zhang and H. Snoussi. (2024), "A multihead attention self-supervised representation model for industrial sensors anomaly detection", *IEEE T Ind. Inform.*, **20**(2), 2190-2199. 10.1109/TII.2023.3280337

Razavian, L., M. Naghipour, M. Shariati and M. Safa. (2020),

"Experimental study of the behavior of composite timber columns confined with hollow rectangular steel sections under compression", *Struct. Eng. Mech.*, **74**(1), 145-156. https://doi.org/10.12989/sem.2020.74.1.145

Rolfe, P. (2012), "Micro- and nanosensors for medical and biological measurement", *Sensors Mater.*, **24**(6), 275-302.

Ruckh, T.T. and H.A. Clark. (2014), "Implantable nanosensors: Toward continuous physiologic monitoring", *Anal. Chem.*, **86**(3), 1314-1323.

Sabetahd, R., S.A. Mousavi Ghasemi, R. Vafaei Poursorkhabi, A. Mohammadzadeh and Y. Zandi. (2022), "Response attenuation of a structure equipped with ATMD under seismic excitations using methods of online simple adaptive controller and online adaptive type-2 neural-fuzzy controller", *Comput. Intell. Neurosci.*, **2022**(1), 5832043. https://doi.org/10.1155/2022/5832043

Safa, M. and V. Kachitvichyanukul. (2019), "Moment rotation prediction of precast beam to column connections using extreme learning machine", *Struct. Eng. Mech.*, **70**(5), 639-647. https://doi.org/10.12989/sem.2019.70.5.639

Safa, M., A. Maleka, M.A. Arjomand, M. Khorami and M. Shariati. (2019), "Strain rate effects on soil-geosynthetic interaction in fine-grained soil", *Geomech. Eng.*, **19**(6), 533-542. https://doi.org/10.12989/gae.2019.19.6.533

Safa, M., P. A. Sari, M. Shariati, M. Suhatril, N.T. Trung, K. Wakil and M. Khorami. (2020), "Development of neuro-fuzzy and neuro-bee predictive models for prediction of the safety factor of eco-protection slopes", *Physica A*, **550**, 124046. https://doi.org/10.1016/j.physa.2019.124046

Safa, M., M. Shariati, Z. Ibrahim, A. Toghroli, S.B. Baharom, N.M. Nor and D. Petković. (2016), "Potential of adaptive neuro fuzzy inference system for evaluating the factors affecting steel-concrete composite beam's shear strength", *Steel Compos. Struct.*, **21**(3), 679-688. http://doi.org/10.12989/scs.2016.21.3.679

Sajedi, F. and M. Shariati. (2019), "Behavior study of NC and HSC RCCs confined by GRP casing and CFRP wrapping", *Steel Compos. Struct*, **30**(5), 417-432. http://doi.org/10.12989/scs.2019.30.5.417

Sedghi, Y., Y. Zandi, M. Shariati, E. Ahmadi, V.M. Azar, A. Toghroli, M. Safa, E.T. Mohamad, M. Khorami and K. Wakil. (2018), "Application of ANFIS technique on performance of C and L shaped angle shear connectors", *Smart Struct. Syst.*, **22**(3), 335-340. http://doi.org/10.12989/sss.2018.22.3.335

Shah, S., N.R. Sulong, M. Jumaat and M. Shariati. (2016), "State-of-the-art review on the design and performance of steel pallet rack connections", *Eng. Fail. Anal.*, **66**, 240-258. https://doi.org/10.1016/j.engfailanal.2016.04.017

Shah, S., N.R. Sulong, R. Khan, M. Jumaat and M. Shariati. (2016), "Behavior of industrial steel rack connections", *Mech. Syst. Signal Proc.*, **70**, 725-740. https://doi.org/10.1016/j.ymssp.2015.08.026

Shah, S., N.R. Sulong, M. Shariati and M. Jumaat. (2015), "Steel rack connections: identification of most influential factors and a comparison of stiffness design methods", *PloS one*, **10**(10), e0139422. https://doi.org/10.1371/journal.pone.0139422

Shah, S., N.R. Sulong, M. Shariati, R. Khan and M. Jumaat. (2016), "Behavior of steel pallet rack beam-to-column connections at elevated temperatures", *Thin Walled Struct.*, **106**, 471-483. https://doi.org/10.1016/j.tws.2016.05.02

Shahabi, S., N. Sulong, M. Shariati and S. Shah. (2016), "Performance of shear connectors at elevated temperatures-A review", *Steel Compos. Struct*, **20**(1), 185-203. https://doi.org/10.12989/scs.2016.20.1.185

Shahabi, S., N.R. Sulong, M. Shariati, M. Mohammadhassani and S. Shah. (2016), "Numerical analysis of channel connectors under fire and a comparison of performance with different types of shear connectors subjected to fire", *Steel Compos. Struct*, **20**(3), 651-669. https://doi.org/10.12989/scs.2016.20.3.651

Shahgoli, A.F., Y. Zandi, A. Heirati, M. Khorami, P. Mehrabi and D. Petkovic. (2020), "Optimisation of propylene conversion response by neuro-fuzzy approach", *Int. J. Hydromechatr.*, **3**(3), 228-237. https://doi.org/10.1504/IJHM.2020.109918

Shariat, M., M. Shariati, A. Madadi and K. Wakil. (2018), "Computational Lagrangian Multiplier Method by using for optimization and sensitivity analysis of rectangular reinforced concrete beams", *Steel Compos. Struct*, **29**(2), 243-256. https://doi.org/10.12989/scs.2018.29.2.243

Shariati, A. (2012), "Various types of shear connectors in composite structures: A review", *Int. J.Phys. Sci.*, **7**(22), http://doi.org/10.18057/IJASC.2021.17.4.8

Shariati, A., N. Sulong, M. Suhatril and M. Shariati. (2012), "Investigation of channel shear connectors for composite concrete and steel T-beam", *Int. J. Phys. Sci.*, **7**(11), 11828-11831. http://doi.org/10.5897/IJPS11.1604

Shariati, M. (2008), "Assessment building using none-destructive test techniques (ultra sonic pulse velocity and Schmidt rebound hammer)", Universiti Putra Malaysia, Malaysia.

Shariati, M. (2013), "Behaviour of C-shaped shear connectors in stell concrete composite beams", Jabatan Kejuruteraan Awam, Fakulti Kejuruteraan, Universiti Malaya, Malaysia.

Shariati, M., D.J. Armaghani, M. Khandelwal, J. Zhou and M. Khorami. (2021), "Assessment of longstanding effects of fly ash and silica fume on the compressive strength of concrete using extreme learning machine and artificial neural network", *J. Adv. Eng. Comput.*, **5**(1), 50-74. http://doi.org/10.25073/jaec.202151.308

Shariati, M., S.M. Azar, M.A. Arjomand, H.S. Tehrani, M. Daei and M. Safa. (2019), "Comparison of dynamic behavior of shallow foundations based on pile and geosynthetic materials in fine-grained clayey soils", *Geomech. Eng.*, **19**(6), 473-484. https://doi.org/10.12989/gae.2020.19.6.473

Shariati, M., S.M. Azar, M.A. Arjomand, H.S. Tehrani, M. Daei and M. Safa. (2020), "Evaluating the impacts of using piles and geosynthetics in reducing the settlement of fine-grained soils under static load", *Geomech. Eng.*, **20**(2), 87-101. https://doi.org/10.12989/gae.2020.20.2.087

Shariati, M., S.M. Davoodnabi, A. Toghroli, Z. Kong and A. Shariati. (2021), "Hybridization of metaheuristic algorithms with adaptive neuro-fuzzy inference system to predict load-slip behavior of angle shear connectors at elevated temperatures", *Compos. Struct.*, **278**, 114524. https://doi.org/10.1016/j.compstruct.2021.114524

Shariati, M., S.S. Faegh, P. Mehrabi, S. Bahavarnia, Y. Zandi, D. R. Masoom, A. Toghroli, N.T. Trung and M.N. Salih. (2019), "Numerical study on the structural performance of corrugated low yield point steel plate shear walls with circular openings", *Steel Compos. Struct.*, **33**(4), 569-581. https://doi.org/10.12989/scs.2019.33.4.569

Shariati, M., M. Ghorbani, M. Naghipour, N. Alinejad and A. Toghroli. (2020), "The effect of RBS connection on energy absorption in tall buildings with braced tube frame system", *Steel Compos. Struct.*, **34**(3), 393-407. https://doi.org/10.12989/scs.2020.34.3.393

Shariati, M., M. Grayeli, A. Shariati and M. Naghipour. (2020), "Performance of composite frame consisting of steel beams and concrete filled tubes under fire loading", *Steel Compos. Struct.*, **36**(5), 587-602. https://doi.org/10.12989/scs.2020.36.5.587

Shariati, M., A. Heyrati, Y. Zandi, H. Laka, A. Toghroli, P. Kianmehr, M. Safa, M.N. Salih and S. Poi-Ngian. (2019), "Application of waste tire rubber aggregate in porous concrete", *Smart Struct. Syst.*, **24**(4), 553-566. http://doi.org/10.12989/sss.2019.24.4.553

Shariati, M., H. Kamyab, M. Habibi, S. Ahmadi, M. Naghipour, F.

Gorjinezhad, S. Mohammadirad and A. Aminian. (2023), "Sulfuric acid resistance of concrete containing coal waste as a partial substitute for fine and coarse aggregates", *Fuel*, **348**, 128311. https://doi.org/10.1016/j.fuel.2023.128311

Shariati, M., M. Lagzian, S. Maleki, A. Shariati and N.T. Trung. (2020), "Evaluation of seismic performance factors for tension-only braced frames", *Steel Compos. Struct.*, **35**(4), 599-609. https://doi.org/10.12989/scs.2020.35.4.599

Shariati, M., M.S. Mafipour, B. Ghahremani, F. Azarhomayun, M. Ahmadi, N.T. Trung and A. Shariati. (2022), "A novel hybrid extreme learning machine–grey wolf optimizer (ELM-GWO) model to predict compressive strength of concrete with partial replacements for cement", *Eng. Comput.*, 1-23. https://doi.org/10.1007/s00366-020-01081-0

Shariati, M., M.S. Mafipour, J.H. Haido, S.T. Yousif, A. Toghroli, N.T. Trung and A. Shariati. (2020), "Identification of the most influencing parameters on the properties of corroded concrete beams using an Adaptive Neuro-Fuzzy Inference System (ANFIS)", *Steel Compos Struct*, **34**(1), 155. https://doi.org/10.12989/scs.2020.34.1.155

Shariati, M., M.S. Mafipour, P. Mehrabi, M. Ahmadi, K. Wakil, N. T. Trung and A. Toghroli. (2020), "Prediction of concrete strength in presence of furnace slag and fly ash using Hybrid ANN-GA (Artificial Neural Network-Genetic Algorithm)", *Smart Struct. Syst.*, **25**(2), 183-195. https://doi.org/10.12989/sss.2020.25.2.183

Shariati, M., M.S. Mafipour, P. Mehrabi, A. Bahadori, Y. Zandi, M.N. Salih, H. Nguyen, J. Dou, X. Song and S. Poi-Ngian. (2019), "Application of a hybrid artificial neural network-particle swarm optimization (ANN-PSO) model in behavior prediction of channel shear connectors embedded in normal and high-strength concrete", *Appl. Sci.*, **9**(24), 5534. https://doi.org/10.3390/app9245534

Shariati, M., M.S. Mafipour, P. Mehrabi, A. Shariati, A. Toghroli, N.T. Trung and M.N. Salih. (2021), "A novel approach to predict shear strength of tilted angle connectors using artificial intelligence techniques", *Eng. Comput.*, **37**, 2089-2109. https://doi.org/10.1007/s00366-019-00930-x

Shariati, M., M.S. Mafipour, P. Mehrabi, Y. Zandi, D. Dehghani, A. Bahadori, A. Shariati, N.T. Trung, M.N. Salih and S. Poi-Ngian. (2019), "Application of Extreme Learning Machine (ELM) and Genetic Programming (GP) to design steel-concrete composite floor systems at elevated temperatures", *Steel Compos. Struct*, **33**(3), 319-332. https://doi.org/10.12989/scs.2019.33.3.319

Shariati, M., M. Naghipour, G. Yousofizinsaz, A. Toghroli and N. P. Tabarestani. (2020), "Numerical study on the axial compressive behavior of built-up CFT columns considering different welding lines", *Steel Compos. Struct.*, **34**(3), 377-391. https://doi.org/10.12989/scs.2020.34.3.377

Shariati, M., M. Raeispour, M. Naghipour, H. Kamyab, A. Memarzadeh, M. Nematzadeh and A. Toghroli. (2024), "Flexural behavior analysis of double honeycomb steel composite encased concrete beams: An integrated experimental and finite element study", *Case Stud. Constr. Mater.*, **20**(e03299. https://doi.org/10.1016/j.cscm.2024.e03299

Shariati, M., S. Rafie, Y. Zandi, R. Fooladvand, B. Gharehaghaj, P. Mehrabi, A. Shariat, N.T. Trung, M.N. Salih and S. Poi-Ngian. (2019), "Experimental investigation on the effect of cementitious materials on fresh and mechanical properties of self-consolidating concrete", *Adv. Concr. Constr.*, **8**(3), 225-237. https://doi.org/10.12989/acc.2019.8.3.225

Shariati, M., N.H. Ramli-Sulong, M.M. Arabnejad, P. Shafigh and H. Sinaei. (2011), "Assessing the strength of reinforced concrete structures through Ultrasonic Pulse Velocity and Schmidt Rebound Hammer tests", *Sci. Res. Essays*, **6**(1), 213-220. https://doi.org/10.5897/SRE10.879

Shariati, M., N. Ramli Sulong and M. Arabnejad Khanouki (2010), "Experimental and analytical study on channel shear connectors in light weight aggregate concrete", *Proceedings of the 4th International Conference on Steel Composite Structures*.

Shariati, M., N. Ramli Sulong, M. Arabnejad Khanouki and A. Shariati (2011), "Experimental and numerical investigations of channel shear connectors in high strength concrete", *Proceedings of the 2011 World Congress on Advances in Structural Engineering And Mechanics* (ASEM'11+).

Shariati, M., N. Ramli Sulong, M. Arabnejad and M. Mahoutian. (2011), "Shear resistance of channel shear connectors in plain, reinforced and lightweight concrete", *Sci. Res. Essays*, **6**(4), 977-983. https://doi.org/10.5897/SRE10.1120

Shariati, M., N. Ramli Sulong, A. Shariati and M. A. Khanouki. (2016), "Behavior of V-shaped angle shear connectors: Experimental and parametric study", *Mater. Struct.*, **49**, 3909-3926. https://doi.org/10.1617/s11527-015-0762-8

Shariati, M., N. Ramli Sulong, M. Suhatril, A. Shariati, M. Arabnejad Khanouki and H. Sinaei (2012), "Fatigue energy dissipation and failure analysis of channel shear connector embedded in the lightweight aggregate concrete in composite bridge girders", *Proceedings of the Fifth International Conference On Engineering Failure Analysis*.

Shariati, M., N.H. Ramli Sulong, H. Sinaei, M.M. Arabnejad Khanouki and P. Shafigh. (2011), "Behavior of channel shear connectors in normal and light weight aggregate concrete (experimental and analytical study)", *Adv. Mater. Res.*, **168**, 2303-2307. https://doi.org/10.4028/www.scientific.net/AMR.168-170.2303

Shariati, M., A. Shariati, N.R. Sulong, M. Suhatril and M.A. Khanouki (2014), *Fatigue energy dissipation and failure analysis of angle shear connectors embedded in high strength concrete*, Elsevier.

Shariati, M., A. Shariati, N.T. Trung, P. Shoaei, F. Ameri, N. Bahrami and S.N. Zamanabadi. (2021), "Alkali-activated slag (AAS) paste: Correlation between durability and microstructural characteristics", *Constr. Build. Mater.*, **267**, 120886. https://doi.org/10.1016/j.conbuildmat.2020.120886

Shariati, M., N.R. Sulong and M.A. Khanouki. (2012), "Experimental assessment of channel shear connectors under monotonic and fully reversed cyclic loading in high strength concrete", *Mater. Des.*, **34**, 325-331. https://doi.org/10.1016/j.matdes.2011.08.008

Shariati, M., N.R. Sulong, A. Shariati and A. Kueh. (2016), "Comparative performance of channel and angle shear connectors in high strength concrete composites: An experimental study", *Constr. Build. Mater.*, **120**, 382-392. https://doi.org/10.1016/j.conbuildmat.2016.05.102

Shariati, M., N.R. Sulong, M. Suhatril, A. Shariati, M.A. Khanouki and H. Sinaei. (2012), "Behaviour of C-shaped angle shear connectors under monotonic and fully reversed cyclic loading: An experimental study", *Mater. Des.*, **41**, 67-73. https://doi.org/10.1016/j.matdes.2012.04.039

Shariati, M., N.R. Sulong, M. Suhatril, A. Shariati, M.A. Khanouki and H. Sinaei. (2013), "Comparison of behaviour between channel and angle shear connectors under monotonic and fully reversed cyclic loading", *Constr. Build. Mater.*, **38**, 582-593. https://doi.org/10.1016/j.conbuildmat.2012.07.050

Shariati, M., M. Tahir, T.C. Wee, S. Shah, A. Jalali, M.A.M. Abdullahi and M. Khorami. (2018), "Experimental investigations on monotonic and cyclic behavior of steel pallet rack connections", *Eng. Fail. Anal.*, **85**, 149-166. https://doi.org/10.1016/j.engfailanal.2017.08.014

Shariati, M., F. Tahmasbi, P. Mehrabi, A. Bahadori and A. Toghroli. (2020), "Monotonic behavior of C and L shaped angle shear connectors within steel-concrete composite beams: an

experimental investigation", *Steel Compos. Struct*, **35**(2), 237-247. https://doi.org/10.12989/scs.2020.35.2.237

Shariati, M., A. Toghroli, A. Jalali and Z. Ibrahim (2017), "Assessment of stiffened angle shear connector under monotonic and fully reversed cyclic loading", *Proceedings of the 5th International Conference on Advances in Civil*, Structural and Mechanical Engineering-CSM.

Shi, G., S. Deng, B. Wang, C. Feng, Y. Zhuang and X. Wang. (2024), "One for all: A unified generative framework for image emotion classification", *IEEE T. Circ. Syst. Video Technol.*, **34**(8), 7057-7068. https://doi.org/10.1109/TCSVT.2023.3341840

Sinaei, H., M.Z. Jumaat and M. Shariati. (2011), "Numerical investigation on exterior reinforced concrete Beam-Column joint strengthened by composite fiber reinforced polymer (CFRP)", *Int. J. Phys. Sci*, **6**(28), 6572-6579. https://doi.org/10.5897/IJPS11.1225

Sinaei, H., M. Shariati, A. H. Abna, M. Aghaei and A. Shariati. (2012), "Evaluation of reinforced concrete beam behaviour using finite element analysis by ABAQUS", *Sci. Res. Essays*, **7**(21), 2002-2009. https://doi.org/10.5897/SRE11.1393

Song, K., H. Yang, D. Liang, L. Chen and M. Jaboyedoff. (2024), "Step-like displacement prediction and failure mechanism analysis of slow-moving reservoir landslide", *J. Hydrol.*, **628**. https://doi.org/10.1016/j.jhydrol.2023.130588

Suhatril, M., N. Osman, P. Azura Sari, M. Shariati and A. Marto. (2019), "Significance of surface eco-protection techniques for cohesive soils slope in Selangor, Malaysia", *Geotech. Geol. Eng.*, **37**, 2007-2014.

Sun, C. and Y. Zhang (2024), "Research on the reliability and path optimization of three-dimensional warehousing vehicles based on genetic-ant colony algorithm", *Proceedings of the 2024 IEEE 2nd International Conference on Sensors*, Electronics and Computer Engineering (ICSECE), IEEE.

Sun, Y. and N. An (2025), "Urban public space design using genetic algorithm and ant colony optimization", *Proceedings of the 2025 International Conference on Intelligent Systems and Computational Networks (ICISCN)*, IEEE.

Taheri, E., S. Esgandarzadeh Fard, Y. Zandi and B. Samali. (2021), "Experimental and numerical investigation of an innovative method for strengthening cold-formed steel profiles in bending throughout finite element modeling and application of neural network based on feature selection method", *Appl. Sci.*, **11**(11), 5242. https://doi.org/10.3390/app11115242

Tahmasbi, F., S. Maleki, M. Shariati, N. Ramli Sulong and M. Tahir. (2016), "Shear capacity of C-shaped and L-shaped angle shear connectors", *PloS one*, **11**(8), e0156989. https://doi.org/10.1371/journal.pone.0156989

Tao, T., G. Li, Y. He and P. Duan. (2019), "Hybrid carbon nanotubes/graphene/nickel fluffy spheres for fast magnetic separation and efficient removal of organic solvents from water", *Mater. Lett.*, **254**, 440-443. https://doi.org/10.1016/j.matlet.2019.06.104

Tavakkoli, O., H. Kamyab, M. Shariati, A.M. Mohamed and R. Junin. (2022), "Effect of nanoparticles on the performance of polymer/surfactant flooding for enhanced oil recovery: A review", *Fuel*, **312**, 122867. https://doi.org/10.1016/j.fuel.2021.122867

Tian, G., J. Tan, B. Li and G. Duan. (2024), "Optimal fully actuated system approach-based trajectory tracking control for robot manipulators", *IEEE T Cybernet.*, **54**(12), 7469-7478. https://doi.org/10.1109/TCYB.2024.3467386

Toghroli, A., P. Mehrabi, M. Shariati, N.T. Trung, S. Jahandari and H. Rasekh. (2020), "Evaluating the use of recycled concrete aggregate and pozzolanic additives in fiber-reinforced pervious concrete with industrial and recycled fibers", *Constr. Build. Mater.*, **252**, 118997. https://doi.org/10.1016/j.conbuildmat.2020.118997

Toghroli, A., M. Mohammadhassani, M. Suhatril, M. Shariati and Z. Ibrahim. (2014), "Prediction of shear capacity of channel shear connectors using the ANFIS model", *Steel Compos Struct*, **17**(5), 623-639. https://doi.org/10.12989/scs.2014.17.5.623

Toghroli, A., M. Shariati, M. Karim and Z. Ibrahim (2017), "Investigation on composite polymer and silica fume–rubber aggregate pervious concrete", *Proceedings of the 5th International Conference on Advances in Civil*, Structural And Mechanical Engineering-CSM.

Toghroli, A., M. Shariati, F. Sajedi, Z. Ibrahim, S. Koting, E.T. Mohamad and M. Khorami. (2018a), "A review on pavement porous concrete using recycled waste materials", *Smart Struct. Syst*, **22**(4), 433-440. https://doi.org/10.12989/sss.2018.22.4.433

Toghroli, A., M. Suhatril, Z. Ibrahim, M. Safa, M. Shariati and S. Shamshirband. (2018b), "Potential of soft computing approach for evaluating the factors affecting the capacity of steel–concrete composite beam", *J. Intell. Manuf.*, **29**, 1793-1801. https://doi.org/10.1007/s10845-016-1217-y

Trung, N.T., N. Alemi, J.H. Haido, M. Shariati, S. Baradaran and S.T. Yousif. (2019), "Reduction of cement consumption by producing smart green concretes with natural zeolites", *Smart Struct. Syst*, **24**(3), 415-425. http://doi.org/10.12989/sss.2019.24.3.415

Vergara, D. (2025), *Voyage Segmentation and Propulsive Power Allocation: A Data-Driven Approach for Short Sea Shipping*, Chalmers Tekniska Hogskola, Sweden. https://doi.org/10.1016/j.joes.2023.11.002

Wan, W., R. Zhang, W. Li, H. Liu, Y. Lin and L. Li. (2016), "Graphene–carbon nanotube aerogel as an ultra-light, compressible and recyclable highly efficient absorbent for oil and dyes", *Environ. Sci. Nano*, **3**(1), 107-113. https://doi.org/10.1039/C5EN00125K

Wang, H., X. Lang and W. Mao. (2021a), "Voyage optimization combining genetic algorithm and dynamic programming for fuel/emissions reduction", *Transp. Res. Part D Transp. Environ.*, **90**, 102670. https://doi.org/10.1016/j.trd.2020.102670

Wang, H., Y. Zandi, M. Gholizadeh and A. Issakhov. (2021b), "Buckling of porosity-dependent bi-directional FG nanotube using numerical method", *Adv. Nano Res.*, **10**(5), 493-507. https://doi.org/10.12989/anr.2021.10.5.493

Wang, J. (2009), "Biomolecule-functionalized nanowires: from nanosensors to nanocarriers", *ChemPhysChem*, **10**(11), 1748-1755. https://doi.org/10.1002/cphc.200900377

Wang, J., Z. Wu, J. Han, G. Wang and S. Lv. (2025a), "Experimental study on axial load-bearing capacity of grout-lifted compressible concrete-filled steel tube composite column", *Tunnell. Undergr. Space Technol.*, **165**, 106864. https://doi.org/10.1016/j.tust.2025.106864

Wang, Y., M. Li, J. Liu, Z. Leng, F.W.B. Li, Z. Zhang and X. Liang. (2025b), "Fg-T2M++: LLMs-augmented fine-grained text driven human motion generation", *Int. J. Comput. Vision*, **133**(7), 4277-4293. https://doi.org/10.1007/s11263-025-02392-9

Wang, Y., Y. Wei, Y. Wei, L. Zhen and S. Deng. (2025c), "Collaborative multidepot split delivery network design with three-dimensional loading constraints", *Transp. Res. Part E Logistics Transp. Rev.*, **196**, 104032. https://doi.org/10.1016/j.tre.2025.104032

Wang, Z., C. Zhang, Z. Chen, W. Hu, K. Lu, L. Ge and Z. Wang. (2024), "ACR-Net: Learning high-accuracy optical flow via adaptive-aware correlation recurrent network", *IEEE T Circ. Syst. Video Technol.*, **34**(10), 9064-9077. https://doi.org/10.1109/TCSVT.2024.3395636

Wei, X., M. Shariati, Y. Zandi, S. Pei, Z. Jin, S. Gharachurlu, M. Abdullahi, M. Tahir and M. Khorami. (2018), "Distribution of shear force in perforated shear connectors", *Steel Compos. Struct.*, **27**(3), 389-399.

https://doi.org/10.12989/scs.2018.27.3.389
Wei, Z., Y. Zandi, M. Gholizadeh, A. Selmi, A. Roco-Videla and U. Konbr. (2021), "On the optimization of building energy, material, and economic management using soft computing", *Adv. Concr. Constr.*, **11**(6), 455-468. https://doi.org/10.12989/acc.2021.11.6.455
Xie, Q. (2019), "An experimental study on the effect of CFRP on behavior of reinforce concrete beam column connections", *Steel Compos. Struct.*, **30**(5), 433-441. https://doi.org/10.12989/scs.2019.30.5.433
Xie, X., A. Gutiérrez, V. Trofimov, I. Szilagyi, T. Soldati and E. Bakker. (2015), "Charged solvatochromic dyes as signal transducers in pH-independent fluorescent and colorimetric ion-selective nanosensors", *Anal. Chem.*, **87**(19), 9954-9959.
Xu, X., C. Qi, X. M. Aretxabaleta, C. Ma, D. Spagnoli and H. Manzano. (2024), "The initial stages of cement hydration at the molecular level", *Nature Commun.*, **15**(1), 2731. https://doi.org/10.1038/s41467-024-46962-w
Yang, H., C. Chen, J. Ni and S. Karekal. (2023), "A hyperspectral evaluation approach for quantifying salt-induced weathering of sandstone", *Sci. Total Environ.*, **885**. https://doi.org/10.1016/j.scitotenv.2023.163886
Yang, H., G. Huang, C. Chen, Y. Yang, Q. Wang and X. Dai. (2024), "Method for evaluation of geological strength index of carbonate cliff rocks: Coupled hyperspectral- digital borehole image technique", *J. Rock Mech. Geotech. Eng.*, **16**(10), 4204-4215. https://doi.org/10.1016/j.jrmge.2024.08.013
Yang, H., L. Qu, L. Chen, K. Song, Y. Yang and Z. Liang. (2024), "Potential sliding zone recognition method for the slow-moving landslide based on the Hurst exponent", *J. Rock Mech. Geotech. Eng.*, **16**, 4105-4124.
Yang, H., K. Song, L. Chen and L. Qu. (2023), "Hysteresis effect and seasonal step-like creep deformation of the Jiuxianping landslide in the Three Gorges Reservoir region", *Eng. Geol.*, **317.** https://doi.org/10.1016/j.enggeo.2023.107089
Yang, L., Y. Gao, H. Chen, H. Jiao, M. Dong, T.A. Bier and M. Kim. (2024), "Three-dimensional concrete printing technology from a rheology perspective: a review", *Adv. Cement Res.*, **36**(12), 567-586. https://doi.org/10.1680/jadcr.23.00205
Yang, T. and T.V. Duncan. (2021), "Challenges and potential solutions for nanosensors intended for use with foods", *Nature Nanotechnol.*, **16**(3), 251-265. https://doi.org/10.1038/s41565-021-00867-7
Yang, X., H. Zhang, Y. Zhuang, Y. Wang, M. Shi and Y. Xu. (2025), "uLiDR: An inertial-assisted unmodulated visible light positioning system for smartphone-based pedestrian navigation", *Inform. Fusion*, **113**, 102579. https://doi.org/10.1016/j.inffus.2024.102579
Yazdani, M., K. Kabirifar, B.E. Frimpong, M. Shariati, M. Mirmozaffari and A. Boskabadi. (2021), "Improving construction and demolition waste collection service in an urban area using a simheuristic approach: A case study in Sydney, Australia", *J. Clean. Prod.*, **280**, 124138. https://doi.org/10.1016/j.jclepro.2020.124138
Zandi, Y., O. Burnaz and A. Durmuş. (2012), "Determining the temperature distributions of fire exposed reinforced concrete cross-sections with different methods", *Res. J. Environ. Earth Sci.*, **4**(8), 782-788. https://doi.org/10.1002/fam.2317
Zandi, Y., M. Shariati, A. Marto, X. Wei, Z. Karaca, D. K. Dao, A. Toghroli, M. H. Hashemi, Y. Sedghi and K. Wakil. (2018), "Computational investigation of the comparative analysis of cylindrical barns subjected to earthquake", *Steel Compos. Struct.*, **28**(4), 439-447. https://doi.org/10.12989/scs.2018.28.4.439
Zhang, C., D. Zhang, M. Zhang, J. Zhang and W. Mao. (2022), "A three-dimensional ant colony algorithm for multi-objective ice routing of a ship in the Arctic area", *Ocean Eng.*, **266**, 113241. https://doi.org/10.1016/j.oceaneng.2022.113241
Zhang, H., X. Xiang, B. Huang, Z. Wu and H. Chen. (2023), "Static homotopy response analysis of structure with random variables of arbitrary distributions by minimizing stochastic residual error", *Comput. Struct.*, **288**, 107153. https://doi.org/10.1016/j.compstruc.2023.107153
Zhao, P., K. Li, N. Zhou, Q. Chen, M. Zhou and C. Qi. (2025), "Enhanced prediction of occurrence forms of heavy metals in tailings: a systematic comparison of machine learning methods and model integration", *Int. J. Miner. Metall. Mater.*, In press. https://doi.org/10.1007/s12613-025-3136-4
Zhao, Y., C. Hu, Y. Hu, H. Cheng, G. Shi and L. Qu. (2012), "A versatile, ultralight, nitrogen-doped graphene framework", *Angewandte Chemie International Edition*, **51**(45), 11371-11375. https://doi.org/10.1002/anie.201206554
Zheng, Y., T. Zhu, J. Chen, K. Shan and J. Li. (2025), "Relationship between pore-size distribution and 1D compressibility of different reconstituted clays based on fractal theory", *Fract. Fraction.*, **9**(4), 235. https://doi.org/10.3390/fractalfract9040235
Ziaei-Nia, A., M. Shariati and E. Salehabadi. (2018), "Dynamic mix design optimization of high-performance concrete", *Steel Compos. Struct.*, **29**(1), 67-75. https://doi.org/10.12989/scs.2018.29.1.067

CC

Nomenclature

Artificial Intelligence	AI
Carbon Nano Tube	CNT
Coefficient of Determination	R^2
Indium Tin Oxide	ITO
Graphene–Carbon Nano Tube	G-CNT
Nano Particles	NPs
Poly Ethylene Terephthalate	PET
Silver Nano Particle	AgNP
Resistance Capacitance	RC
Energy-Dispersive X-ray Spectroscopy	EDS
Finite Element Method	FEM
Root Mean Square	RMS
Signal-to-Noise Ratio	SNR
Printed Circuit Board	PCB
Scanning Electron Microscope	SEM
Graphene Nano Platelets	GNPs
Multi-Walled Carbon Nano Tubes	MWCNTs

Digital Image Correlation	DIC
Convolutional Recurrent Neural Network	CRNN
Long Short-Term Memory	LSTM
Power Spectral Density	PSD
Finite Element Analysis	FEA
Electric Currents	EC
Solid Mechanics	SM
One At a Time	OAT
Serial Peripheral Interface – Direct Memory Access	SPI-DMA
Mean Time-To-Update	MTTU
Minimum Detectable Pressure	MDP
Poly Vinyli Dene Fluoride	PVDF
Full Scale Output	FSO
Chemical Vapor Deposition	CVD